Yewdell, J.W., 1999. Intracellular localization of proteasomal degradation of a viral antigen. J. Cell. Biol. 146, 113–124.

Boutell, L.M., Thomas, P., Neal, J.W., Weston, V.J., Duce, J., Harper, P.S., Jones, A.L., 1999. Aberrant interactions of transcriptional repressor proteins with the Huntington's disease gene product, huntingtin. Hum. Mol. Genet. 8, 1647–1655.

Chai, Y., Koppenhafer, S.L., Shoesmith, S.J., Perez, M.K., Paulson, H.L., 1999. Evidence for proteasome involvement in polyglutamine disease: Localization to nuclear inclusions in SCA3/MJD and suppression of polyglutamine aggregation in vitro. Hum. Mol. Genet. 8, 673–682.

Chai, Y., Wu, L., Griffin, J.D., Paulson, H.L., 2001. The role of protein composition in specifying nuclear inclusion formation in polyglutamine disease. J. Biol. Chem. 276, 44889–44897.

Cummings, C.J., Mancini, M.A., Antalffy, B., DeFranco, D.B., Orr, H.T., Zoghbi, H.Y., 1998. Chaperone suppression of aggregation and altered subcellular proteasome localization imply protein misfolding in SCA1. Nat. Genet. 19, 148–154.

Cummings, C.J., Reinstein, E., Sun, Y., Antalffy, B., Jiang, Y., Ciechanover, A., Orr, H.T., Beaudet, A.L., Zoghbi, H.Y., 1999. Mutation of the E6-AP ubiquitin ligase reduces nuclear inclusion frequency while accelerating polyglutamine-induced pathology in SCA1 mice. Neuron 24, 879–892.

Daniel, M.T., Koken, M., Romagne, O., Barbey, S., Bazarbachi, A., Stadler, M., Guillemin, M.C., Degos, L., Chomienne, C., de Thé, H., 1993. PML protein expression in hematopoietic and acute promyelocytic leukemia cells. Blood 82, 1858–1867.

Dundr, M., Misteli, T., 2001. Functional architecture in the cell nucleus. Biochem. J. 356, 297–310.

Everett, R.D., Meredith, M., Orr, A., Cross, A., Kathoria, M., Parkinson, J., 1997. A novel ubiquitin-specific protease is dynamically associated with the PML nuclear domain and binds to a herpesvirus regulatory protein. Embo. J. 16, 519–530.

Freemont, L.S., 2000. RING for destruction. Curr. Biol. 10, R84–87.

Fujigasaki, H., Martin, J.J., De Deyn, P.P., Camuzat, A., Deffond, D., Stevanin, G., Dermaut, B., Van Broeckhoven, C., Dürr, A., Brice, A., 2001. CAG repeat expansion in the TATA box-binding protein gene causes autosomal dominant TATA box-binding protein gene causes autosomal dominant cerebellar ataxia. Brain 124, 1939–1947.

Fujigasaki, H., Uchihara, T., Koyano, S., Iwabuchi, K., Yagishita, S., Makifuchi, T., Nakamura, A., Ishida, K., Toru, S., Hirai, S., Ishikawa, K., Tanabe, T., Mizusawa, H., 2000. Ataxin-3 is translocated into the nucleus for the formation of intranuclear inclusions in normal and Machado-Joseph disease brains. Exp. Neurol. Dis. 65, 248–256.

Kaytor, M.D., Durick, L.A., Skinner, P.J., Koob, M.D., Ranum, L.P., Orr, H.T., 1999. Nuclear localization of the spinocerebellar ataxia type 7 protein, ataxin-7. Hum. Mol. Genet. 8, 1657–1664.

Khan, M.M., Nomura, T., Kim, H., Kaul, S.C., Wadhwa, R., Shinagawa, T., Ichikawa-Iwata, E., Zhong, S., Pandolfi, P.P., Ishii, S., 2001. Role of PML and PML-RARalpha in Mad-mediated transcriptional repression. Mol. Cell 7, 1233–1243.

Klement, I.A., Skinner, P.J., Kaytor, M.D., Yi, H., Hersch, S.M., Clark, H.B., Zoghbi, H.Y., Orr, H.T., 1998. Ataxin-I nuclear localization and aggregation: role in polyglutamine-induced disease in SCA1 transgenic mice. Cell 95, 41–53.

Kuemmerle, S., Gutekunst, C.A., Klein, A.M., Li, X.J., Li, S.H., Beal, M.F., Hersch, S.M., Ferrante, R.J., 1999. Huntington aggregates may not predict Ferrante R.J. 1999 Huntington aggregates may not predict neuronal death in Huntington's disease. Ann. Neurol. 46, 842–849.

Lallemand-Breitenbach, V., Zhu, J., Puvion, F., Koken, M., Honore, N., Doubeikovsky, A., Duprez, E., Pandolfi, P.P., Puvion, E., Freemont, P., de The, H., 2001. Role of promyelocytic leukemia (PML) sumolation in nuclear body formation, 11S proteasome recruitment, and As203-induced PML or PML/retinoic acid receptor alpha degradation. J. Exp. Med. 193, 1361–1371.

Mattsson, K., Pokrovskaja, K., Kiss, C., Klein, G., Szekely, L., 2001. Proteins associated with the promyelocytic leukemia gene product (PML)-containing nuclear body move to the nucleolus upon inhibition of proteasome-dependent protein degradation. Proc. Natl. Acad. Sci. USA 98, 1012–1017.

McCampbell, A., Taylor, J.P., Taye, A.A., Robitschek, J., Li, M., Walcott, J., Merry, D., Chai, Y., Paulson, H., Sobue, G., Fischbeck, K.H., 2000. CREB-binding protein sequestration by expanded polyglutamine. Hum. Mol. Genet. 9, 2197–2202.

Nakamura, K., Jeong, S.Y., Uchihara, T., Anno, M., Nagashima, K., Nagashima, T., Ikeda, S., Tsuji, S., Kanazawa, I., 2001. SCA17, a novel autosomal dominant cerebellar ataxia caused by an expanded polyglutamine in TATA-binding protein. Hum. Mol. Genet. 10, 1441–1448.

Nucifora Jr., F.C., Sasaki, M., Peters, M.F., Huang, H., Cooper, J.K., Yamada, M., Takahashi, H., Tsuji, S., Troncoso, J., Dawson, V.L., Dawson, T.M., Ross, C.A., 2001. Interference by huntingtin and atrophin-1 with cbp-mediated transcription leading to cellular toxicity. Science 291, 2423–2428.

Reyes, J.C., 2001. PML and COP1—two proteins with much in common. Trends Biochem. Sci. 26, 18–20.

Ross, C.A., Margolis, R.L., Becher, M.W., Wood, J.D., Engelender, S., Cooper, J.K., Sharp, A.H., 1998. Pathogenesis of neurodegenerative diseases associated with expanded glutamine repeats: new answers, new questions. Prog. Brain Res. 117, 397–419.

Saudou, F., Finkbeiner, S., Devys, D., Greenberg, M.E., 1998. Huntingtin acts in the nucleus to induce apoptosis but death does not correlate with the formation of intranuclear inclusions. Cell 95, 55–66.

Seeler, J.S., Dejean, A., 1999. The PML nuclear bodies: Actors or extras. Curr. Opin. Genet. Dev. 9, 362–367.

Shimohata, T., Nakajima, T., Yamada, M., Uchida, C., Onodera, O., Naruse, S., Kimura, T., Koide, R., Nozaki, K., Sano, Y., Ishiguro, H., Sakoe, K., Ooshima, T., Sato, A., Ikeuchi, T., Oyake, M., Sato, T., Aoyagi, Y., Hozumi, I., Nagatsu, T., Takiyama, Y., Nishizawa, M., Goto, J., Kanazawa, I., Davidson, I., Tanese, N., Takahashi, H., Tsuji, S., 2000. Expanded polyglutamine stretches interact with TAFII130, interfering with CREB-dependent transcription. Nat. Genet. 26, 29–36.

Shimohata, T., Onodera, O., Tsuji, S., 2001. Expanded polyglutamine stretches lead to aberrant transcriptional regulation in polyglutamine diseases. Hem. Cell 14, 17–25.

Skinner, C.J., Koshy,, F.T., Cummings, C.J., Klement, I.A., Helin, K., Servadio, A., Zoghbi, H.Y., Orr, H.T., 1997. Ataxin-1 with an expanded glutamine tract alters nuclear matrix-associated structures. Nature 389, 971–974.

Steffan, J.S., Kazantsev, A., Spasic-Boskovic, O., Greenwald, M., Zhu, Y.Z., Gohler, H., Wanker, E.E., Bates, G.P., Housman, D.E., Thompson, L.M., 2000. The Huntington's disease protein interacts with p53 and CREB-binding protein and represses transcription. Proc. Natl. Acad. Sci. USA 97, 6763–6768.

Stenoien, D.L., Cummings, C.J., Adams, H.P., Mancini, M.G., Patel, K., DeMartino, G.N., Marcelli, M., Weigel, N.L., Mancini, M.A., 1999. Polyglutamine-expanded androgen receptors form aggregates that sequester heat shock proteins, proteasome components and SRC-1, and are suppressed by the HDJ-2 chaperone. Hum. Mol. Genet. 8, 731–741.

Tait, D., Riccio, M., Sittler, A., Scherzinger, E., Santi, S., Ognibene, A., Maraldi, N.M., Lehrach, H., Wanker, E.E., 1998. Ataxin-3 is transported into the nucleus and associates with the nuclear matrix. Hum. Mol. Genet. 7, 991–997.

Takahashi, J., Fujigasaki, H., Zander, C., El Hachimi, K.H., Stevanin, G., Durr, A., Lebre, A.S., Yvert, G., Trottier, Y., de Thé, H., Hauw, J.J., Duyckaerts, C., Brice, A., 2002. Two populations of neuronal intranuclear inclusions in SCA7 differ in size and PML content. Brain 125, 1534–1543.

Wood, J.D., Nucifora Jr., F.C., Duan, K., Zhang, C., Wang, J., Kim, Y., Schilling, G., Sacchi, N., Liu, J.M., Ross, C.A., 2000. Atrophin-1, the dentato-rubral and pallido-luysian atrophy gene product, interacts with ETO/MTG8 in the nuclear matrix and represses transcription. J. Cell Biol. 150, 939–948.

Wyttenbach, A., Carmichael, J., Swartz, J., Furlong, R.A., Narain, Y., Rankin, J., Rubinsztein, D.C., 2000. Effects of heat shock, heat shock

protein 40 (HDJ-2), and proteasome inhibition on protein aggregation in cellular models of Huntington's disease. Proc. Natl. Acad. Sci. USA 97, 2898–2903.

Yamada, M., Sato, T., Shimohata, T., Hayashi, S., Igarashi, S., Tsuji, S., Takahashi, H., 2001a. Interaction between neuronal intranuclear inclusions and promyelocytic leukemia protein nuclear and coiled bodies in CAG repeat diseases. Am. J. Pathol. 159, 1785–1795.

Yamada, M., Wood, J.D., Shimohata, T., Hayashi, S., Tsuji, S., Ross, C.A., Takahashi, H., 2001b. Widespread occurrence of intranuclear atrophin-1 accumulation in the central nervous system neurons of patients with dentatorubral-pallidoluysian atrophy. Ann. Neurol. 49, 14–23.

Yvert, G., Lindenberg, K.S., Picaud, S., Landwehrmeyer, G.B., Sahel, J.A., Mandel, J.L., 2000. Expanded polyglutamines induce neurodegeneration and trans-neuronal alterations in cerebellum and retina of SCA7 transgenic mice. Hum. Mol. Genet. 9, 2491–2506.

Zhang, S., Xu, L., Lee, J., Xu, T., 2002. Drosophila atrophin homolog functions as a transcriptional corepressor in multiple developmental processes. Cell 108, 45–56.

Zhong, S., Salomoni, P., Pandolfi, P.P., 2000. The transcriptional role of PML and the nuclear body. Nat. Cell Biol. 2, E85–90.

Zhu, J., Lallemand-Breitenbach, V., de Thé, H., 2001. Pathways of retinoic acid-or arsenic trioxide-induced PML/RARalpha catabolism, role of oncogene degradation in disease remission. Oncogene 20, 7257–7265.

Zoghbi, H.Y., Orr, H.T., 2000. Glutamine repeats and neurodegeneration. Annu. Rev. Neurosci. 23, 217–247.

Acta Neuropathol (2003) 106 : 436–440
DOI 10.1007/s00401-003-0740-z

REGULAR PAPER

Kazuko Aoki · Toshiki Uchihara · Ayako Nakamura
Takashi Komori · Nobutaka Arai · Toshio Mizutani

Expression of apolipoprotein E in ballooned neurons – Comparative immunohistochemical study on neurodegenerative disorders and infarction

Received: 14 April 2003 / Revised: 10 June 2003 / Accepted: 10 June 2003 / Published online: 24 July 2003
© Springer-Verlag 2003

Abstract Apolipoprotein E (ApoE) in neurons is suggested to play crucial roles in neuronal degeneration and regeneration. We used antibodies against ApoE and phosphorylated neurofilament (pNF) to investigate the immunohistochemical features of ballooned neurons (BNs) in infarction and in various chronic degenerative disorders, including Pick body disease, corticobasal degeneration/progressive supranuclear palsy, Alzheimer's disease, and frontotemporal dementia. BNs in these chronic degenerative processes were intensely labeled with the anti-pNF as reported, whereas BNs in infarction showed less intense pNF-like immunoreactivity (IR). In addition, BNs in infarction were characterized by an intense ApoE-like IR. This ApoE-like IR was inconsistent or less intense in BNs in the chronic degenerative processes. The rarity of ApoE-positive glial cells in the vicinity of ApoE-positive BNs suggests that accumulated ApoE in BNs is generated in the neurons. Accumulation of ApoE in BNs in infarction may be linked to a regenerative process after acute transection of axons, which seems compromised in chronic degenerative processes.

K. Aoki · T. Uchihara (✉) · A. Nakamura
Department of Neuropathology,
Tokyo Metropolitan Institute for Neuroscience,
2-6 Musashi-dai, Fuchu, 183-8526 Tokyo, Japan
Tel.: +81-42-3253881 ext 4712, Fax: +81-42-3218678,
e-mail: uchihara@tmin.ac.jp

K. Aoki
Department of Neurology,
Metropolitan Fuchu Medical Center
for Severe Motor and Intellectual Disabilities,
2-9-2 Musashi-dai, Fuchu, 183-0042 Tokyo, Japan

T. Komori · N. Arai
Department of Clinical Neuropathology,
Tokyo Metropolitan Institute for Neuroscience,
2-6 Musashi-dai, Fuchu, 183-8526 Tokyo, Japan

T. Mizutani
Department of Pathology,
Tokyo Metropolitan Neurological Hospital,
2-6-1 Musashi-dai, Fuchu, 183-0042 Tokyo, Japan

Keywords Apolipoprotein E · Ballooned neuron · Immunohistochemistry · Neurodegenerative disease · Infarction

Introduction

Ballooned neurons (BNs) are histological features with abundant homogeneous cytoplasm and eccentrically placed nuclei, observed in several neurodegenerative diseases of the central nervous system (CNS), such as Pick body disease (PBD) [6, 30, 44], corticobasal degeneration (CBD) [28, 36, 43], Creutzfeldt-Jakob disease (CJD) [6, 17, 31], Alzheimer's disease (AD) [6, 9], progressive supranuclear palsy (PSP) [22, 29] and several other diseases [7, 15, 19, 27, 37]. They are most frequent in cortical layers III, V and VI, and are easily identifiable on hematoxylin and eosin (HE)-stained preparations as pale-stained swollen neurons, often with a surrounding artifactual area of vacuolation [21]. Ultrastructurally, the cytoplasm of BNs is filled with numerous straight or slightly curved filaments of 10–14 nm or 25–30 nm in diameter that were interspersed among vesicular profiles, granular material, mitochondria, and lipofuscin bodies [2, 19, 28, 30, 43].

Several comparative immunohistochemical studies on BNs have demonstrated that immunoreactivity (IR) of αB-crystallin [7, 16, 20, 29] and that of phosphorylated neurofilament (pNF) proteins [9, 15, 19, 28, 29, 31, 33, 39] are commonly observed in BNs in several neurodegenerative diseases. It is suggested that impaired axoplasmic transport involving neurofilaments might be a possible underlying mechanism shared among various dementing neurodegenerative diseases [9]. It remains to be settled whether this hypothesis can be extrapolated to BNs in cerebral infarction, another condition associated with appearance of BNs. Lowe et al. [20] reported that ubiquitin-like IR, prominent in BNs of neurodegenerative diseases, was absent in BNs of infarction, suggesting that underlying mechanism of neuronal swelling might vary according to the conditions.

Apolipoprotein E (ApoE) is synthesized in various organs including the brain [23] and is a predominant apo-

lipoprotein in the brain. The cellular source of ApoE in the CNS was initially considered to be restricted to astrocytes [4, 35], but recent investigations showed neuronal expression of ApoE in both neurodegenerative and stable physiological conditions [1, 11, 12, 24]. ApoE is supposed to play several roles according to the conditions [1, 11, 12, 24, 32, 41, 42], and has been reported to play a role in repair of the CNS [13, 14, 23, 40]. Parallel in vitro study on cultured cell line corroborated these in vivo findings [8, 25, 26, 34]. This prompted us to investigate a possible role of ApoE in the formation of BNs in various pathological conditions.

Materials and methods

Cases

Brains from 10 cases with cerebral infarction, 3 with CBD/PSP, 2 with frontotemporal dementia (FTD), 1 with PBD, and 1 with AD were enrolled in this study. Each diagnosis was based on both clinical history and postmortem neuropathological verification. These 17 cases were selected after the identification of numerous BNs on HE-stained sections. Clinical data are summarized in Table 1. Appearance of BNs in infarction was restricted to cases with ischemic involvement of the subcortical white matter with relative preservation of the cerebral cortex itself. Because most of the ischemic foci linked to BNs were not large enough to identify the relevant clinical event, the exact date of ischemia for each ischemic lesion was not readily traceable from the clinical record.

Immunohistochemistry

Formalin-fixed, paraffin-embedded blocks that included the cortical area with BNs were cut at 5-μm thickness. Sections were deparaffinized, treated in a microwave oven in citrate buffer three times for 5 min, treated with 1% hydrogen peroxide for 30 min, and incubated for 2 days at 4°C either with ApoEAB947 [38] (1:2,000, anti-human recombinant ApoE; Chemicon, Temecula, CA), ApoEC (1:2,000, anti-human ApoE polyclonal antibody raised against a synthetic peptide EKVQAAVGTSAAPVPSDNH equivalent to the C-terminal amino acid sequence 299–317 of human ApoE; IBL, Gunma, Japan) or SMI31 (1:10,000, anti-pNF antibody; Sternberger monoclonal, Baltimore, MD) diluted with phosphate-buffered saline (PBS) containing 0.03% Triton X-100 and the corresponding blocking serum. The sections were then incubated for 2 h with a biotinylated secondary antibody (1:1,000, Vector, Burlingame, CA), followed by avidin-biotin-peroxidase complex (1:1,000, ABC Elite, Vector). The peroxidase labeling was visualized with diaminobenzidine and nickel ammonium sulfate as chromogen, which yielded a dark purple reaction product.

For further characterization of BNs, double-immunofluorescence staining for ApoE and pNF, with the same antibodies used for the previous single staining, was performed and, the relationship between ApoE-like IR and pNF-like IR was assessed. Deparaffinized sections were incubated with ApoEAB947 (1:200) and SMI31 (1:1,000) for 2 days at 4°C. The sections were incubated with biotinylated anti-goat IgG (1:1000, Vector), the secondary antibody for ApoEAB947, for 2 h and then fluorolabeled with fluorescein isothiocyanate (FITC) conjugated with streptavidin (1:200, Vector) for ApoE, and Rhodamine Red-X-conjugated anti-mouse IgG (1:200, Jackson Immunoresearch laboratories, West Grove, PA) for SMI31. The FITC and rhodamine signals were observed under the fluorescence microscope combined with a laser confocal system (TCS-SP, Leica, Heidelberg, Germany), and the images were captured and recorded on magneto-optical disks. The same sections were then subjected to HE staining to confirm that the immunopositive cells were BNs, and the already photographed immunopositive neurons were identified using various structures such as lipofuscin granules and blood vessels as landmarks.

Table 1 Summary of clinical data (*PBD* Pick body disease, *CBD* corticobasal degeneration, *AD* Alzheimer's disease, *PSP* progressive surpranuclear palsy, *FTD* frontotemporal dementia, *MI* multiple infarction, *E* embolism, *Y* years, *D* days, *F* frontal cortex, *T* temporal cortex)

Case	Age at death (years)	Sex	Diagnosis	Disease duration	Section
1	77	F	CBD	8 Y	F
2	64	M	CBD	4 Y	F
3	65	F	PSP	10 Y	F
4	75	M	FTD	7 Y	T
5	72	M	FTD	13 Y	F
6	69	M	PBD	13 Y	F
7	66	F	AD	3 Y	F
8	81	M	MI	Unknown	F
9	68	F	E	14 D	F
10	69	M	MI	Unknown	F
11	75	F	MI	Unknown	T
12	85	M	MI	Unknown	F
13	68	F	MI	Unknown	F
14	84	F	MI	Unknown	T
15	80	F	MI	Unknown	F
16	90	M	MI	Unknown	T
17	67	M	E	2 D	F

Results

More than 340 BNs in cases with infarction and more than 140 BNs in cases with neurodegenerative diseases were observed. The two polyclonal antibodies against ApoE (ApoEC and ApoEAB947) gave essentially identical results. BNs in infarction, in all the cases examined, exhibited an intense ApoE-like IR (Fig. 1A). In neurodegenerative diseases, this ApoE-like IR in BNs was absent or less intense (Fig. 1B, C). pNF-like IR was variably present in the BNs in all cases examined (Fig. 1D–F), although it was less intense in BNs in infarction (Fig. 1D). As representative cases of neurodegenerative diseases, BNs in AD (Fig. 1B, E) and PBD (Fig. 1C, F) are shown; the same immunohistochemical features (scarce ApoE-like IR and intense pNF-like IR) were shared among BNs in other neurodegenerative diseases. In the AD case, ApoE IR was observed clearly in senile plaques, but rarely in BNs (Fig. 1B). In cases of infarction, ApoE-positive glial cells were rarely observed where ApoE accumulated in BNs (Fig. 1A). In addition to BNs, ApoE IR was observed in neurons around ischemic foci, as we reported previously [1].

Double immunofluorescence for ApoE (green, labeled with FITC) and pNF (red, labeled with rhodamine) confirmed the above findings and further clarified relationship between ApoE and pNF in BNs (Fig. 2A–C). ApoE-like IR (labeled with FITC) was predominant in BNs in infarction, while pNF-like IR (labeled with rhodamine) was less

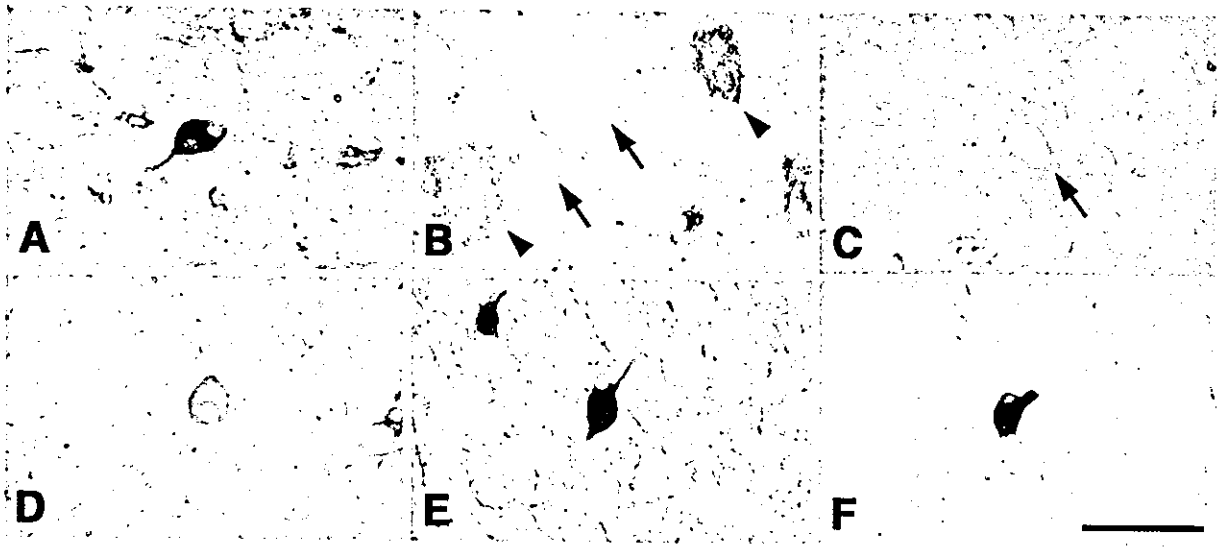

Fig. 1 Immunohistochemical features of BNs. ApoE-like IR (**A–C**) and pNF IR (**D–F**) in BNs in infarction (**A, D**), AD (**B, E**) and PBD (**C, F**) are shown. BNs in infarction exhibit an intense ApoE-like IR (**A**), but those (**B, C**, *arrows*) in neurodegenerative diseases rarely exhibit ApoE-like IR, whereas pNF-like IR is, in contrast, less intense in BNs in infarction (**D**) than those in neurodegenerative diseases (**E, F**). In the AD case (**B**), ApoE-like IR is observed clearly in senile plaques (*arrowheads*), but rarely in BNs (*arrows*). In cases of infarction, ApoE-positive glial cells are rarely observed in regions where ApoE is accumulated in BNs (**A**) (*BNs* ballooned neurons, *ApoE* apolipoprotein E, *IR* immunoreactivity, *pNF* phosphorylated neurofilament, *AD* Alzheimer's disease, *PBD* Pick body disease). *Bar* 50 μm

intense in these BNs (Fig. 2A). In contrast, ApoE-like IR was not evident in BNs in chronic degenerative diseases (Fig. 2B, C), e.g., in AD, where prominent pNF-like IR in BNs was not accompanied by ApoE-like IR, although senile plaques near the BNs were immunopositive for ApoE (Fig. 2B). Colocalization of these two epitopes in BNs was observed frequently in cases of infarction. This colocalization was, however, rare in chronic neurodegenerative processes, because of the paucity of ApoE-like IR in these neurons. ApoE-positive glial cells were rarely observed where ApoE accumulated in BNs in infarction. Each swollen neuron (arrows in Fig. 2A–C), fluoropositive for either ApoE or pNF was confirmed as a BN after staining the same microscopic field with HE (arrows in Fig. 2D–F).

Discussion

BNs in neurodegenerative disorders are considered to share a common underlying mechanism for their formation [9]. We wanted to clarify whether BNs in infarction also shared

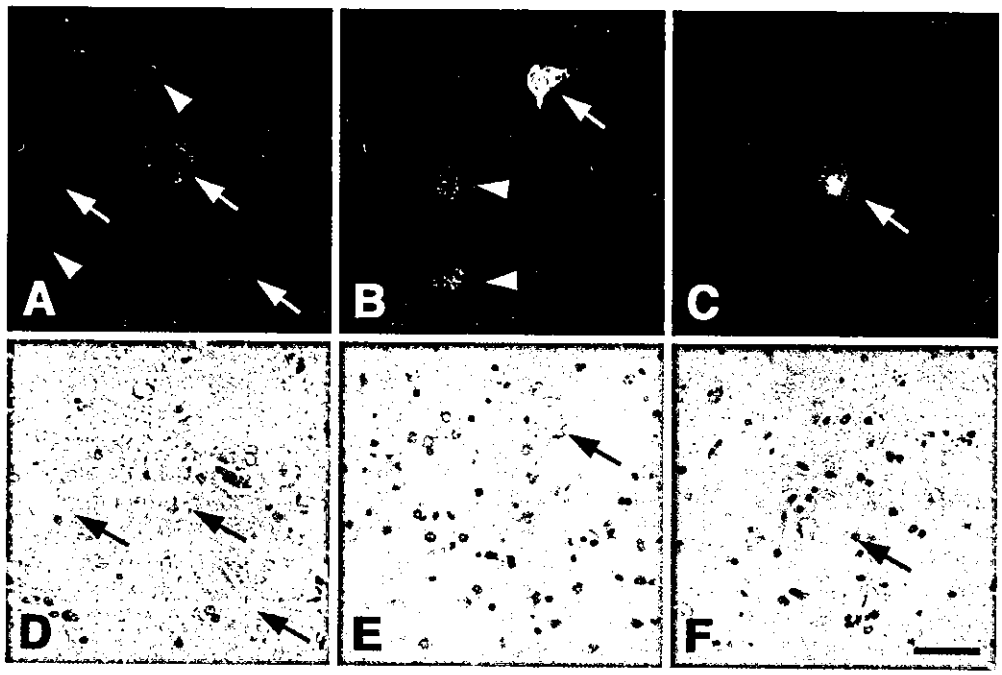

Fig. 2 Double-labeling immunofluorescence and HE staining of BNs. Double-labeling images stained for ApoE (FITC, *green*) and pNF (rhodamine, *red*) were recorded and the same section was then subjected to HE staining. Double-labeling immunofluorescence (**A–C**) and the same microscopic field on HE staining (**D–F**) are shown (**A, D** infarction; **B, E** AD; **C, F** PBD). ApoE-like IR is present variably in the BNs of infarction (**A**; *arrows*), whereas it is not evident in BNs of other neurodegenerative diseases (**B, C**; *arrows*). Positive ApoE-like IR in senile plaques (**B**, *arrowhead*) verified successful ApoE immunostaining, whereas BNs (**B**, *arrows*) are negative for ApoE in the AD case. ApoE-positive glial cells are only rare in regions where ApoE accumulates in BNs, but vessels are ApoE positive in infarction (**A**, *arrowheads*). *Bar* 50 μm

a similar mechanism, and found that pNF accumulated in BNs in infarction, as in chronic degenerative processes [9, 15, 19, 28, 29, 31, 33, 39]. Neuronal accumulation of ApoE was, however, restricted to BNs in infarction and not evident in chronic degenerative processes, regardless of the diagnoses. This is in contrast with ubiquitin-like IR in BNs, which is positive in chronic neurodegenerative diseases and negative in infarction, but further corroborated the hypothesis that cellular mechanism for formation of BNs may be different in infarction [20].

One of the hypotheses to explain accumulation of pNF in BNs is axonal disruption that potentially leads to stagnated axonal flow and cytoplasmic accumulation of pNF to form BNs [9, 19]. This well explains the frequent appearance of BNs in relatively intact cortical area with an ischemic lesion in the subjacent white matter, as demonstrated in the present study. Although it remains to be clarified whether the accumulation of pNF in chronic neurodegenerative processes is induced by disruption of axon, as seen in infarction, or by other mechanisms [18, 31, 39], the accumulation of ApoE in BNs is another distinguishing features of infarction not observed in chronic degenerative processes. Because ApoE-positive glial cells were rare in the vicinity of these BNs, it is difficult to suppose that ApoE is generated extraneuronally and internalized into BNs. Alternatively, ApoE could be produced in neurons as reported [1, 11, 12, 24], and this accumulation may represent one of the cellular reactions after axonal disruption. Indeed, ApoE has been considered to play a crucial role in neurite extension and regeneration [13, 14, 23, 40]. Isoform-dependent effects of ApoE further support this hypothesis [5]. Furthermore, the absence of ApoE-like IR in some tau-immunopositive neurons suggests that ApoE plays a secondary role in neurofibrillary tangle (NFT) formation, or is accumulated within neurons in response to reparative process induced by NFT-associated neuronal damage [3]. If the surviving neurons with disrupted axons still remain sufficiently active after acute ischemic attack, it is reasonable to suppose that their regenerative mechanism takes place during the recovery period by expressing ApoE. In contrast, neurons in chronic degenerative processes may be so compromised by some long-lasting insult that they are no longer capable of running their regenerative mechanism properly. This would explain the paucity of ApoE-like IR in BNs, which is common to chronic degenerative processes.

The present study demonstrates the discrepancy between pNF and ApoE epitopes in BNs of different pathological conditions. Although ApoE and some cytoskeletal proteins, including neurofilaments, potentially interact with each other [10], this discrepancy suggests that participation of ApoE and its interaction with NF proteins are not prerequisite for the formation of BNs in general. ApoE is presumably involved in regeneration of neurons and neurites, because it is observed not only in BNs but also in neurons around ischemic focus without cytoplasmic swelling or pNF-like IR. Because the distribution of ApoE-positive BNs was different from ApoE-positive neurons without ballooning in ischemic brain, it is probable that neuronal accumulation of ApoE is related to different mechanisms, axonal disruption and neuronal ischemia itself. However, it is very likely that ApoE is involved in neuronal regeneration in both types of ApoE-positive neurons, a process not necessarily related to neurofilament proteins.

This study raises the possibility that ApoE protein functions as a mediator of neuronal regeneration after ischemia, although the exact molecular mechanisms leading to neuronal loss after ischemia remain elusive and could be multiple. One of the ways to construct reasonable therapeutic strategies may be to characterize the major pathways leading to neuronal death, such as oxidative stress, which are, however, still too complicated to dissect. One may otherwise concentrate on molecules, such as ApoE, which are known to have possible regenerative activities. How they are expressed in different pathological conditions may provide essential clues to understanding their functions and pathological relevance in human brains, and lead to therapeutic strategies for various neurological disorders including both neurodegeneration and ischemia.

References

1. Aoki K, Uchihara T, Sanjo N, Nakamura A, Ikeda K, Tsuchiya K, Wakayama Y (2003) Increased expression of neuronal apolipoprotein E in human brain with cerebral infarction. Stroke 34:875–880
2. Arima K, Uesugi H, Fujita I, Sakurai Y, Oyanagi S, Andoh S, Izumiyama Y, Inose T (1994) Corticonigral degeneration with neuronal achromasia presenting with primary progressive aphasia: ultrastructural and immunocytochemical studies. J Neurol Sci 127:186–197
3. Benzing WC, Mufson EJ (1995) Apolipoprotein E immunoreactivity within neurofibrillary tangles: relationship to tau and PHF in Alzheimer's disease. Exp Neurol 132:162–171
4. Boyles JK, Pitas RE, Wilson E, Mahley RW, Taylor JM (1985) Apolipoprotein E associated with astrocytic glia of the central nervous system and with nonmyelinating glia of the peripheral nervous system. J Clin Invest 76:1501–1513
5. Buttini M, Orth M, Bellosta S, Akeefe H, Pitas RE, Wyss-Coray T, Mucke L, Mahley RW (1999) Expression of human apolipoprotein E3 or E4 in the brains of *Apoe*$^{-/-}$ mice: isoform-specific effects on neurodegeneration. J Neurosci 19:4867–4880
6. Clark AW, Manz HJ, White III CL, Lehmann J, Miller D, Coyle JT (1986) Cortical degeneration with swollen chromatolytic neurons: its relationship to Pick's disease. J Neuropathol Exp Neurol 45:268–284
7. Cooper PN, Jackson M, Lennox G, Lowe J, Mann DMA. (1995) τ, ubiquitin, and αB-crystallin immunohistochemistry define the principal causes of degenerative frontotemporal dementia. Arch Neurol 52:1011–1015
8. Dekroon RM, Armati PJ (2001) Synthesis and processing of apolipoprotein E in human brain cultures. Glia 33:298–305
9. Dickson DW, Yen S-H, Suzuki KI, Davies P, Garcia JH, Hirano A (1986) Ballooned neurons in select neurodegenerative diseases contain phosphorylated neurofilament epitopes. Acta Neuropathol (Berl) 71:216–223
10. Fleming LM, Weisgraber KH, Strittmatter WJ, Troncoso JC, Johnson GVW (1996) Differential binding of apolipoprotein E isoforms to tau and other cytoskeletal proteins. Exp Neurol 138: 252–260

11. Han S-H, Einstein G, Weisgraber KH, Strittmatter WJ, Saunders AM, Pericak-Vance M, Roses AD, Schmechel DE (1994) Apolipoprotein E is localized to the cytoplasm of human cortical neurons: a light and electron microscopic study. J Neuropathol Exp Neurol 53:535–544
12. Han S-H, Hulette C, Saunders AM, Einstein G, Pericak-Vance M, Strittmatter WJ, Roses AD, Schmechel DE (1994) Apolipoprotein E is present in hippocampal neurons without neurofibrillary tangles in Alzheimer's disease and in age-matched controls. Exp Neurol 128:13–26
13. Horsburgh K, Nicoll JAR (1996) Selective alterations in the cellular distribution of apolipoprotein E immunoreactivity following transient cerebral ischaemia in the rat. Neuropathol Appl Neurobiol 22:342–349
14. Horsburgh K, Kelly S, McCulloch J, Higgins GA, Roses AD, Nicoll JAR (1999) Increased neuronal damage in apolipoprotein E-deficient mice following global ischaemia. Neuroreport 10:837–841
15. Kato S, Hirano A (1990) Ubiquitin and phosphorylated neurofilament epitopes in ballooned neurons of the extraocular muscle nuclei in a case of Werdnig-Hoffmann disease. Acta Neuropathol 80:334–337
16. Kato S, Hirano A, Umahara T, Kato M, Herz F, Ohama E (1992) Comparative immunohistochemical study on the expression of αB crystallin, ubiquitin and stress-response protein 27 in ballooned neurons in various disorders. Neuropathol Appl Neurobiol 18:335–340
17. Kato S, Hirano A, Umahara T, Llena JF, Herz F, Ohama E (1992) Ultrastructural and immunohistochemical studies on ballooned cortical neurons in Creutzfeldt-Jakob disease: expression of αB-crystallin, ubiquitin and stress-response protein 27. Acta Neuropathol 84:443–448
18. Lee VM-Y, Otvos L, Carden MJ, Hollosi M, Dietzschold B, Lazzarini RA (1988) Identification of the major multiphosphorylation site in mammalian neurofilaments. Proc Natl Acad Sci USA 85:1998–2002
19. Lippa CF, Smith TW, Fontneau N (1990) Corticonigral degeneration with neuronal achromasia: a clinicopathologic study of two cases. J Neurol Sci 98:301–310
20. Lowe J, Errington DR, Lennox G, Pike I, Spendlove I, Landon M, Mayer RJ (1992) Ballooned neurons in several neurodegenerative diseases and stroke contain αB crystallin. Neuropathol Appl Neurobiol 18:341–350
21. Lowe J, Lennox G, Leigh PN (1997) Disorders of movement and system degenerations. In: Graham DI, Lantos PL (eds) Greenfield's neuropathology, 6th edn. Arnold, London, pp 281–366
22. Mackenzie IRA, Hudson LP (1995) Achromatic neurons in the cortex of progressive supranuclear palsy. Acta Neuropathol 90: 615–619
23. Mahley RW (1988) Apolipoprotein E: cholesterol transport protein with expanding role in cell biology. Science 240:622–630
24. Metzger RE, LaDu MJ, Pan JB, Getz GS, Frail DE, Falduto MT (1996) Neurons of the human frontal cortex display apolipoprotein E immunoreactivity: implications for Alzheimer's disease. J Neuropathol Exp Neurol 55:372–380
25. Michikawa M, Fan Q-W, Isobe I, Yanagisawa K (2000) Apolipoprotein E exhibits isoform-specific promotion of lipid efflux from astrocytes and neurons in culture. J Neurochem 74: 1008–1016
26. Michikawa M, Gong J-S, Fan Q-W, Sawamura N, Yanagisawa K (2001) A novel action of Alzheimer's amyloid β-protein (Aβ): oligomeric Aβ promotes lipid release. J Neurosci 21: 7226–7235
27. Mizutani T, Inose T, Nakajima S, Gambetti P (1993) Familial Parkinsonism and dementia with "ballooned neurons". Adv Neurol 60:613–617
28. Mori H, Nishimura M, Namba Y, Oda M (1994) Corticobasal degeneration: a disease with widespread appearance of abnormal tau and neurofibrillary tangles, and its relation to progressive supranuclear palsy. Acta Neuropathol 88:113–121
29. Mori H, Oda M, Mizuno Y (1996) Cortical ballooned neurons in progressive supranuclear palsy. Neurosci Lett 209:109–112
30. Murayama S, Mori H, Ihara Y, Tomonaga M (1990) Immunocytochemical and ultrastructural studies of Pick's disease. Ann Neurol 27:394–405
31. Nakazato Y, Hirato J, Ishida Y, Hoshi S, Hasegawa M, Fukuda T (1990) Swollen cortical neurons in Creutzfeldt-Jakob disease contain a phosphorylated neurofilament epitope. J Neuropathol Exp Neurol 49:197–205
32. Namba Y, Tomonaga M, Kawasaki H, Otomo E, Ikeda K (1991) Apolipoprotein E immunoreactivity in cerebral amyloid deposits and neurofibrillary tangles in Alzheimer's disease and kuru plaque amyloid in Creutzfeldt-Jakob disease. Brain Res 541:163–166
33. Paulus W, Selim M (1990) Corticonigral degeneration with neuronal achromasia and basal neurofibrillary tangles. Acta Neuropathol 81:89–94
34. Pitas RE, Boyles JK, Lee SH, Foss D, Mahley RW (1987) Astrocytes synthesize apolipoprotein E and metabolize apolipoprotein E-containing lipoproteins. Biochim Biophys Acta 917: 148–161
35. Poirier J, Hess M, May PC, Finch CE (1991) Astrocytic apolipoprotein E mRNA and GFAP mRNA in hippocampus after entorhinal cortex lesioning. Mol Brain Res 11:97–106
36. Rebeiz JJ, Kolodny EH, Richardson EP (1968) Corticodentatonigral degeneration with neuronal achromasia. Arch Neurol 18:20–33
37. Schmidt ML, Carden MJ, Lee VM-Y, Trojanowski JQ (1987) Phosphate dependent and independent neurofilament epitopes in the axonal swelling of patients with motor neuron disease and controls. Lab Invest 56:282–294
38. Schwab C, Steele JC, Akiyama H, McGeer PL (1996) Distinct distribution of apolipoprotein E and β-amyloid immunoreactivity in the hippocampus of Parkinson dementia complex of Guam. Acta Neuropathol 92:378–385
39. Smith TW, Lippa CF, Girolami U (1992) Immnocytochemical study of ballooned neurons in cortical degeneration with neuronal achromasia. Clin Neuropathol 11:28–35
40. Snipes GJ, McGuire CB, Norden JJ, Freeman JA (1986) Nerve injury stimulates the secretion of apolipoprotein E by nonneuronal cells. Proc Natl Acad Sci USA 83:1130–1134
41. Stoll G, Mueller HW, Trapp BD, Griffin JW (1989) Oligodendrocytes but not astrocytes express apolipoprotein E after injury of rat optic nerve. Glia 2:170–176
42. Uchihara T, Duyckaerts C, He Y, Kobayashi K, Seilhean D, Amouyel P, Hauw J-J (1995) ApoE immunoreactivity and microglial cells in Alzheimer's disease brain. Neurosci Lett 195: 5–8
43. Wakabayashi K, Oyanagi K, Makifuchi T, Ikuta F, Homma A, Homma Y, Horikawa Y, Tokiguchi S (1994) Corticobasal degeneration: etiopathological significance of the cytoskeletal alterations. Acta Neuropathol 87:545–553
44. Williams HW (1935) The peculiar cells of Pick's disease: their pathogenesis and distribution in disease. Arch Neurol Psychiatry 34:508–519

Acta Neuropathol (2003) 106 : 121–124
DOI 10.1007/s00401-003-0709-y

REGULAR PAPER

Kazuko Aoki · Toshiki Uchihara · Kuniaki Tsuchiya
Ayako Nakamura · Kenji Ikeda · Yoshihiro Wakayama

Enhanced expression of aquaporin 4 in human brain with infarction

Received: 2 January 2003 / Revised: 20 March 2003 / Accepted: 20 March 2003 / Published online: 25 April 2003
© Springer-Verlag 2003

Abstract A series of human brains with cerebral infarction obtained at autopsy were investigated to clarify the possible contribution of aquaporin 4 (AQP4) to the development of brain edema. Cellular localization of AQP4 and its relation to ischemic foci were examined with double-labeling immunohistochemistry. AQP4 immunoreactivity (IR) was more intense at the periphery of ischemic foci than at their center. Double-labeling study demonstrated that AQP4 IR was restricted to astrocytes and was localized to their entire processes, including their end feet facing the outer surface of capillaries. Moreover, AQP4 IR, detectable in the subpial and subependymal zone in the normal condition, was more intense in the vicinity of ischemic foci. Accumulation of AQP4 IR may reflect its participation in the development of brain edema in human brains by playing a role in the transport of water not only through blood vessel walls but also through pial and ependymal surface of the brain.

K. Aoki · T. Uchihara (✉) · A. Nakamura
Department of Neuropathology,
Tokyo Metropolitan Institute for Neuroscience,
2-6 Musashi-dai, Fuchu, 183-8526 Tokyo, Japan
Tel.: +81-42-3253881 ext. 4712, Fax: +81-42-3218678,
e-mail: uchihara@tmin.ac.jp

K. Aoki · Y. Wakayama
Department of Neurology, Showa University Fujigaoka Hospital,
1-30 Fujigaoka, Aoba-ku, 227-8501 Yokohama, Japan

K. Aoki
Department of Neurology,
Metropolitan Fuchu Medical Center for Severe Motor
and Intellectual Disabilities,
2-9-2 Musashi-dai, Fuchu, 183-0042 Tokyo, Japan

K. Tsuchiya
Department of Laboratory Medicine and Pathology,
Tokyo Metropolitan Matsuzawa Hospital,
2-1-1 Kamikitazawa, Setagaya-ku, 156-8585 Tokyo, Japan

K. Ikeda
Department of Psychogeriatrics, Tokyo Institute of Psychiatry,
2-1-8 Kamikitazawa, Setagaya-ku, 156-8585 Tokyo, Japan

Keywords Aquaporin 4 · Ischemia · Glia · Brain edema · Osmotic regulation

Introduction

Aquaporin (AQP) family of water channel proteins is present on the plasma membrane at the boundary of various tissues and is supposed to regulate water balance at the interface between different tissues. AQP4, AQP1 and other AQP subtypes have been identified in the central nervous system [17]. Although the distribution of AQP1 is restricted to the choroid plexus [11], AQP4 is present in cells lining the subarachnoid space and ventricles in normal unaffected brains [2, 3, 5, 12, 16]. While experimental data suggest that AQP4 is involved in the development of brain edema [13, 18], it remains to be established how the expression of AQP4 is altered after pathological insults in human brains. If AQP4 plays a role in the development of brain edema, one may expect that its localization and expression may be altered in the vicinity of ischemic lesions. This prompted us to examine localization and intensity of AQP4 immunoreactivity (IR) in human brains with cerebral infarction.

Materials and methods

Brains from seven patients with ischemic foci (dating from 8 days to 10 months before autopsy, age at death: 49–93 years) were examined in this study. Demographic data of these patients are shown in Table 1. Written consent to undertake autopsy was obtained from the responsible family members of the patients. Formalin-fixed, paraffin-embedded blocks, including both the area of ischemic necrosis and the surrounding nonnecrotic area, were prepared. Immunohistochemistry was performed using an anti-AQP4 antibody (1:10,000) raised against the peptide (CEKKGKDSSGEVLSSV) homologous to the C-terminal end of the cytoplasmic domain of the rat AQP4. The specificity of the antibody, which cross-reacts with human AQP4, has been established previously [7]. The epitope was visualized with the avidin-biotin-peroxidase complex (ABC Elite kit, Vector, Burlingame, CA) method with diaminobenzidine and nickel ammonium sulfate as a chromogen to yield a deep purple reaction product. To specify cellular localiza-

Table 1 Summary of clinical data. The major foci of ischemia corresponding to the fatal ischemic attack are shown (*Age* age at death, *Interval* time from onset of ischemic attack to death, *Lt* left, *F* frontal lobe, *Rt* right, *MCA* middle cerebral artery, *P* parietal lobe, *O* occipital lobe)

Case	Age (years)	Sex	Interval	Ischemic lesion
1	93	F	8 days	Lt F
2	69	M	8 days	Rt MCA
3	89	F	11 days	Rt P, O
4	68	F	13 days	Lt F, P
5	66	F	14 days	Rt F
6	49	M	7 months	Rt F, P
7	77	F	10 months	Rt F, P, O

tion of AQP4, these AQP4-immunostained sections were subjected to the second-cycle immunostaining either with anti-human glial fibrillary acidic protein (GFAP) antibody (1:1,000, Dako, Glostrup, Denmark) or with biotinylated *Ricinus communis* agglutinin (RCA, 1:1,000, Seikagakukogyo, Tokyo, Japan), a marker for endothelial cells and microglia. The procedure for the second-cycle immunostaining was essentially the same as the first-cycle, except for omission of nickel ammonium sulfate from the chromogen to yield a brown reaction product.

Results

AQP4 IR in the area free from ischemic changes was mainly restricted to the subpial (Fig. 1A), and subependymal (Fig. 1B) zone. Less intense AQP4 IR was detectable around the vessels (Fig. 1C), as reported in normal rat brains [2, 3, 5, 12, 16]. AQP4 IR was readily detectable in the vicinity of the ischemic lesion (Fig. 2A) and was more intense at the periphery (arrowheads, Fig. 2A) of the lesion than at the center (asterisk, Fig. 2A). This AQP4 IR was more pronounced in recent foci than in older foci seen by chance on the same section. Influence of the interval between the ischemic attack and autopsy on AQP4 IR was, however, not readily apparent when compared between the cases. Double labeling of the ischemic foci with the anti-AQP4 and the anti-GFAP antibodies (Fig. 2A, B, E–G), demonstrated that AQP4 IR was abundant as dots (arrowheads, Fig. 2B) along the entire foot processes and their end feet of GFAP-positive cells. It was detectable also in the cell body (Fig. 2B). Double-labeled sections with the anti-AQP4 antibody and biotinylated RCA (Fig. 2C, D, H) demonstrated that these RCA-positive cells lacked AQP4 IR (Fig. 2C, D). At the center of ischemic legions, surviving cellular components were not so abundant and rarely exhibited AQP4 IR (asterisk, Fig. 2A). AQP4 IR in the center of ischemic foci was not intense, and restricted to glial cells of astrocytic morphology around capillaries, even when detectable (Fig. 2E). An increase in AQP4 IR near ischemic foci was also apparent in subpial zone (Fig. 2F) and subependymal zone (Fig. 2G) as well as in perivascular area (Fig. 2H).

Discussion

An experimental occlusion of the middle cerebral artery of rat demonstrated that edematous area at the periphery of the induced ischemic lesion, monitored by magnetic resonance imaging, was rich in AQP4 mRNA [14], while the precise immunolocalization of AQP4 remains undefined. Moreover, data on immunolocalization of AQP4 in human brain have not been available up to now. In the present study, we demonstrated that AQP4 protein accumulated at the periphery of ischemic foci of human brain. Furthermore, the double-labeling study demonstrated that AQP4 was localized exclusively to astrocytes, most of which had close contact with capillaries through their foot processes. Although it has been reported that AQP4 mRNA and AQP4 IR could be detectable in blood vessels isolated from rat brain [6] or perivascular astrocytes [12, 16], another study reported that AQP4 mRNA was exclusively detectable in cultured astrocytes prepared from rat cerebral cortex, but not in cultured oligodendrocytes, microglia or neurons [19]. Our immunohistochemical study demonstrated that astrocytes were the only cellular com-

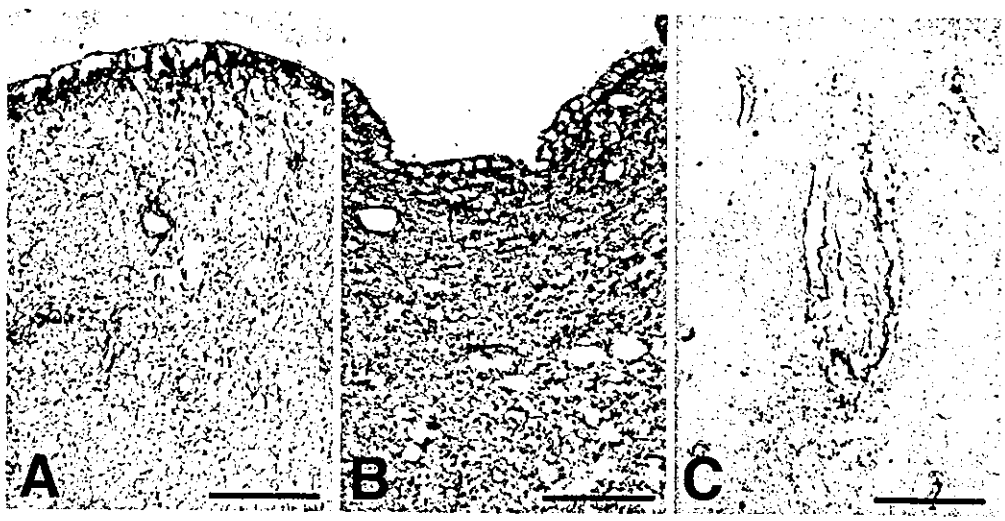

Fig. 1 Immunolocalization of AQP4 in an area distant from ischemic foci. Double immunolabeling for AQP4 (*purple*) and GFAP (*brown*) (**A**, **B**), and AQP4 (*purple*) and RCA (*brown*) (**C**). In these areas free from ischemic changes, AQP4 IR is restricted to subpial zone (**A**) and subependymal zone (**B**). Less intense AQP4 IR is also detectable around the blood vessel (**C**) (*AQP4* Aquaporin 4, *RCA Ricinus communis* agglutinin, *IR* immunoreactivity). *Bars* A–C 50 μm

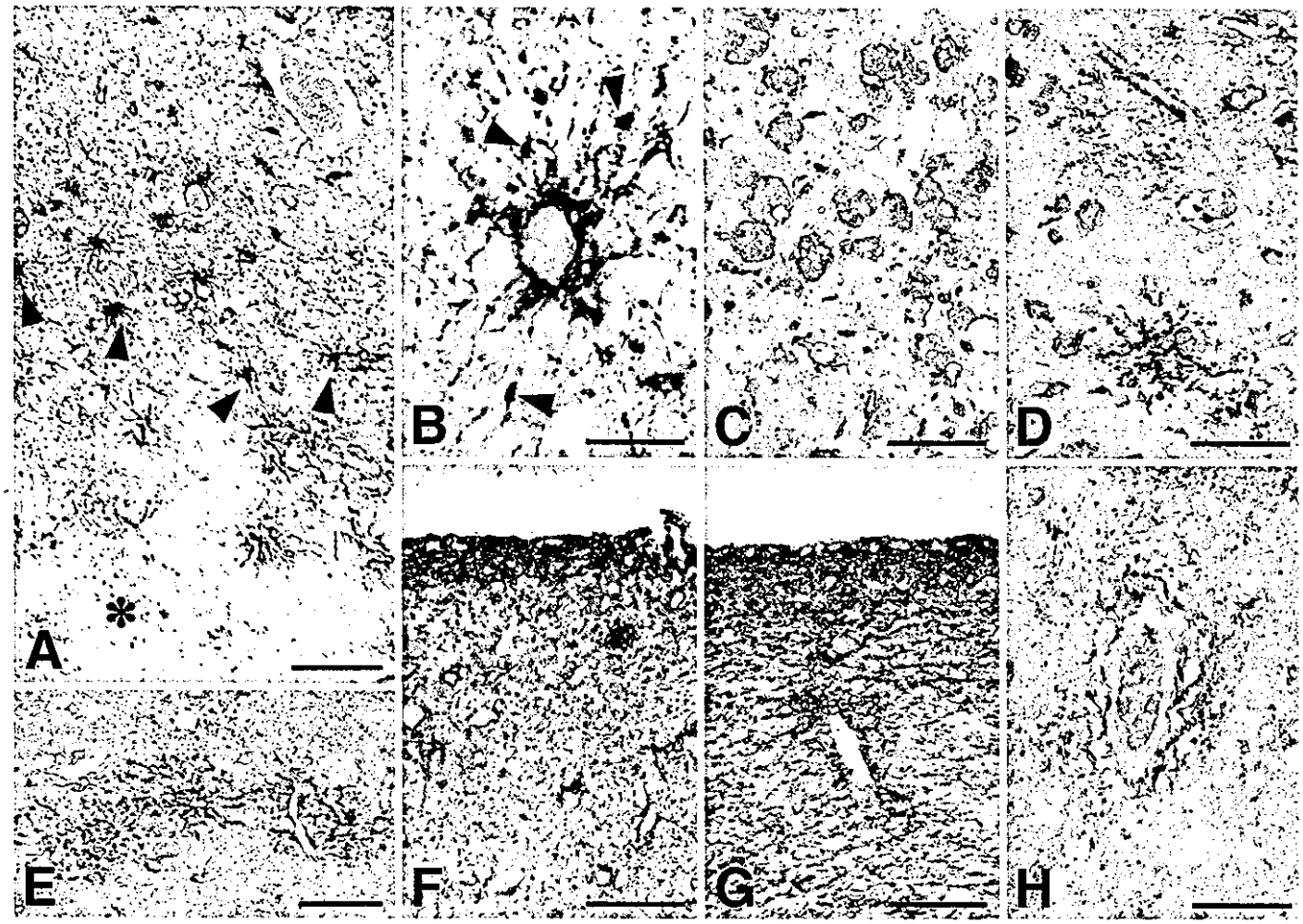

Fig. 2 Immunolocalization of AQP4 in and around ischemic foci. Double immunolabeling of AQP4 (*purple*) and GFAP (*brown*) (**A**, **B**, **E–G**), and AQP4 (*purple*) and RCA lectin (*brown*) (**C**, **D**, **H**). **A** AQP4 IR is readily detectable in the vicinity of the ischemic foci and more abundant at the periphery (*upper half, arrowheads*) of the lesion than in its center (*lower half, asterisk*). **B** AQP4 IR is present as dots (*arrowheads*) along the entire processes and in the cell body of GFAP-positive cells). **C**, **D** No AQP4 IR is detectable in the cells positive for RCA. **E** At the center of less severe legions, AQP4 IR is restricted to glial cells of astrocytic morphology around the capillaries. **F–H** Near the ischemic foci, AQP4 IR is also increased at the subpial zone (**F**), and subependymal zone (**G**), as well as around the blood vessels (**H**). *Bars* **A** 100 μm; **B** 20 μm; **C–H** 50 μm

ponent that express AQP4 in ischemic foci of human brain. One study [15] demonstrated an increase in AQP4 IR even in experimentally induced hyponatremia, even when the blood-brain barrier (BBB) remained intact. Because the osmolality of the brain tissue exceeds that of the serum at an early phase of brain ischemia [4], expression of AQP4 in astrocytes might have been triggered by this gradient in osmolality. This is corroborated by the finding that the Na^+-K^+-Cl^- cotransporter, potentially involved in electrolyte balance, is co-localized with AQP4 to processes of perivascular astrocytes [20]. These findings suggest that the expression of AQP4 is initially triggered by this change in metabolic environment, and its up-regulation is related to compensation of this gradient in osmolality by transporting water into the brain tissue. Continued expression of AQP4 even after disruption of the BBB may potentially exacerbate subsequent brain edema. This hypothesis is compatible with what we observed on human brains, and was confirmed by an experimental study demonstrating that development of brain edema was greatly attenuated in mice whose AQP4 gene was deleted [9].

AQP4 was also expressed in subpial and subependymal regions of unaffected area in human brains (Fig. 1A, B, respectively), as shown in normal rat brains [2, 3, 5, 12, 16]. Because these two areas are at the interface between the cerebrospinal fluid (CSF) and the brain tissue, it is speculated that AQP4 present in these area is also involved in the transport of water between CSF and the brain tissue even under normal physiological conditions [2, 3, 5, 12, 16]. Interestingly, expression of AQP4 in these areas was also increased when these areas were included in or very close to the ischemic foci. If this increase in expression of AQP4 in these areas is related to acceleration of water transport, as speculated around the blood vessels, this will provide another route for water transport through the pial and ependymal surface of the brain, which may potentially exacerbate brain edema.

Although it is currently considered that AQP4 is one of the major molecules involved in the development of brain edema around ischemic foci [14] and neoplasm [13], another molecule in the AQP family, AQP9, has been reported

to be present in astrocytes around ischemic foci, suggesting that AQP4 and AQP9 are synergistic during development of brain edema [1]. However, enhanced expression of AQP4 is not restricted to brain edema. It becomes detectable in chick optic tectum at embryonic day 9 and thereafter [10], although the functional significance of this finding remains speculative, because mice deprived of the AQP4 gene develop without apparent abnormalities except for a slight decrease in the ability to concentrate urine [8]. Moreover, AQP4 mRNA could be up-regulated after experimental insults other than ischemia, such as exogenous neurotoxins or mechanical transection [18]. Up-regulation of AQP4 in these situations not directly related to brain edema raises the possibility that AQP4 may be involved in functions other than exacerbating brain edema. Indeed, AQP4 IR was still detectable around ischemic foci even after the brain edema had already resolved (for case 7, 10 months after the ischemic attack).

This immunohistochemical study clarified, for the first time in the human brains with ischemia, that AQP4 was up-regulated in astrocytes, which had a close contact with capillaries. This up-regulation was also found in subpial and subependymal areas close to ischemic foci. Because these areas (pericapillary, subpial and subependymal) are at the interface to the body fluids, it is speculated that AQP4 in these areas are commonly involved in the transport of water under not only physiological but also pathological conditions. These observations will be of help in understanding the development of brain edema and in establishing therapeutic strategies aimed at reducing brain edema by modifying the expression of AQP4.

References

1. Badaut J, Hirt L, Granziera C, Bogousslavsky J, Magistretti PJ, Regli L (2001) Astrocyte-specific expression of aquaporin-9 in mouse brain is increased after transient focal cerebral ischemia. J Cereb Blood Flow Metab 21:477–482
2. Frigeri A, Gropper MA, Turck CW, Verkman AS (1995) Immunolocalization of the mercurial-insensitive water channel and glycerol intrinsic protein in epithelial cell plasma membranes. Proc Natl Acad Sci USA 92:4328–4331
3. Hasegawa H, Ma T, Skach W, Matthay MA, Verkman AS (1994) Molecular cloning of a mercurial-insensitive water channel expressed in selected water-transporting tissues. J Biol Chem 269:5497–5500
4. Hatashita S, Hoff JT, Salamat SM (1988) Ischemic brain edema and the osmotic gradient between blood and brain. J Cereb Blood Flow Metab 8:552–559
5. Jung JS, Bhat RV, Preston GM, Guggino WB, Baraban JM, Agre P (1994) Molecular characterization of an aquaporin cDNA from brain: candidate osmoreceptor and regulator of water balance. Proc Natl Acad Sci USA 91:13052–13056
6. Kobayashi H, Minami S, Itoh S, Shiraishi S, Yokoo H, Yanagita T, Uezono Y, Mohri M, Wada A (2001) Aquaporin subtypes in rat cerebral microvessels. Neurosci Lett 297:163–166
7. Liu JW, Wakayama Y, Inoue M, Shibuya S, Kojima H, Jimi T, Oniki H (1999) Immunocytochemical studies of aquaporin 4 in the skeletal muscle of mdx mouse. J Neurol Sci 164:24–28
8. Ma T, Yang B, Gillespie A, Carlson EJ, Epstein CJ, Verkman AS (1997) Generation and phenotype of a transgenic knockout mouse lacking the mercurial-insensitive water channel aquaporin-4. J Clin Invest 100:957–962
9. Manley GT, Fujimura M, Ma T, Noshita N, Filiz F, Bollen AW, Chan P, Verkman AS (2000) Aquaporin-4 deletion in mice reduces brain edema after acute water intoxication and ischemic stroke. Nat Med 6:159–163
10. Nico B, Frigeri A, Nicchia GP, Quondamatteo F, Herken R, Errede M, Ribatti D, Svelto M, Roncali L (2001) Role of aquaporin-4 water channel in the development and integrity of the blood-brain barrier. J Cell Sci 114:1297–1307
11. Nielsen S, Smith BL, Christensen EI, Agre P (1993) Distribution of the aquaporin CHIP in secretory and resorptive epithelia and capillary endothelia. Proc Natl Acad Sci USA 90:7275–7279
12. Nielsen S, Nagelhus EA, Amiry-Moghaddam M, Bourque C, Agre P, Ottersen OP (1997) Specialized membrane domains for water transport in glial cells: high-resolution immunogold cytochemistry of aquaporin-4 in rat brain. J Neurosci 17:171–180
13. Saadoun S, Papadopoulos MC, Davies DC, Krishna S, Bell BA (2002) Aquaporin-4 expression is increased in oedematous human brain tumours. J Neurol Neurosurg Psychiatry 72:262–265
14. Taniguchi M, Yamashita T, Kumura E, Tamatani M, Kobayashi A, Yokawa T, Maruno M, Kato A, Ohnishi T, Kohmura E, Tohyama M, Yoshimine T (2000) Induction of aquaporin-4 water channel mRNA after focal ishemia in rat. Mol Brain Res 78:131–137
15. Vajda Z, Promeneur D, Dóczi T, Sulyok E, Frøkiaer J, Ottersen OP, Nielsen S (2000) Increased aquaporin-4 immunoreactivity in rat brain in response to systemic hyponatremia. Biochem Biophys Res Commun 270:495–503
16. Venero JL, Vizuete ML, Ilundain AA, Machado A, Echevarria M, Cano J (1999) Detailed localization of aquaporin-4 messenger RNA in the CNS: preferential expression in periventricular organs. Neuroscience 94:239–250
17. Venero JL, Vizuete ML, Machado, A Cano J (2001) Aquaporins in the central nervous system. Prog Neurobiol 63:321–336
18. Vizuete ML, Venero JL, Vargas C, Ilundain AA, Echevarria M, Machado A, Cano J (1999) Differential upregulation of aquaporin-4 mRNA expression in reactive astrocytes after brain injury: potential role in brain edema. Neurobiol Dis 6: 245–258
19. Yamamoto N, Yoneda K, Asai K, Sobue K, Toda T, Fujita Y, Katsuya H, Fujita M, Aihara N, Mase M, Yamada K, Miura Y, Kato T (2001) Alterations in the expression of the AQP family in cultured rat astrocytes during hypoxia and reoxygenation. Mol Brain Res 90:26–38
20. Yan Y, Dempsey RJ, Sun D (2001) Expression of Na^+-K^+-Cl^- cotransporter in rat brain during development and its localization in mature astrocytes Brain Res 911:43–55

Reprinted from JOURNAL OF NEUROLOGY, NEUROSURGERY & PSYCHIATRY, May 2003, Vol 74, No 5, p 597-601

PAPER

Attenuated nuclear shrinkage in neurones with nuclear inclusions of SCA1 brains

U Nagaoka, T Uchihara, K Iwabuchi, H Konno, M Tobita, N Funata, S Yagishita, T Kato

J Neurol Neurosurg Psychiatry 2003;74:597–601

See end of article for authors' affiliations

Correspondence to: Dr T Uchihara, Department of Neuropathology, Tokyo Metropolitan Institute for Neuroscience, 2-6 Musashidai, Fuchu, Tokyo 183-8526, Japan; uchihara@tmin.ac.jp

Received 20 June 2002
In revised form 12 November 2002
Accepted 21 November 2002

Background: Spinocerebellar ataxia type 1 (SCA1) is one of the autosomal dominant neurodegenerative disorders commonly linked to pathological expansion of the CAG repeat of the relevant gene. Nuclear inclusions and neurodegeneration are both triggered by this pathological expansion of the CAG/polyglutamine repeat on ataxin-1, but it remains to be determined whether or not nuclear inclusion formation is associated with accelerated neurodegeneration.
Objective: To examine the influence of nuclear inclusions on nuclear size and deformity in human brains from patients suffering from SCA1.
Material: Pontine sections of brains obtained at necropsy from seven patients with SCA1 and five controls.
Methods: The size and deformity of each neuronal nucleus was quantified. Nuclei with and without inclusions were examined separately to assess the possible influence of nuclear inclusions on neurodegeneration.
Results: Nuclear shrinkage and deformity were more marked in SCA1 brains than in controls. This shrinkage was attenuated in neurones containing nuclear inclusions.
Conclusions: The existence of nuclear inclusions in SCA1 is presumably linked to a mechanism that attenuates rather than accelerates nuclear shrinkage. This in vivo finding may provide a clue to constructing a rational therapeutic strategy for combating neurodegeneration associated with nuclear inclusions.

Spinocerebellar ataxia type 1 (SCA1) is an autosomal dominant neurodegenerative disorder characterised by degeneration of the cerebellar Purkinje cells, inferior olive neurones, and neurones within cranial nerve nuclei, leading to progressive ataxia, dysarthria, amyotrophy, and bulbar dysfunction. Symptoms of SCA1 typically become apparent in mid-life and worsen over the subsequent 10 to 15 years. The mutations of the gene linked to SCA1 and several other autosomal dominant neurodegenerative disorders have been shown to be an expansion of the CAG trinucleotide repeat which results in an abnormally elongated polyglutamine tract in the mutated proteins. The normal alleles of the SCA1 gene contain up to 36 CAG repeats, whereas disease alleles have over 43 repeats.[1]

Numerous studies have suggested that the expanded polyglutamine tract leads to neurodegeneration by conferring a toxic gain of function rather than by loss of normal physiological function. One of the hallmarks of these diseases is the formation of insoluble protein aggregates or inclusions, which are found in the brains of affected patients. The inclusions are immunoreactive for ubiquitin and contain expanded polyglutamine, molecular chaperones, and components of the proteasome.[2 3] Therefore, it is assumed that these CAG/polyglutamine repeat disorders share a mechanism underlying nuclear inclusion formation and neurodegeneration, both being triggered by an expansion of CAG/polyglutamine. How the expanded polyglutamine leads to long term neurodegeneration, however, remains unknown, and one of the essential questions is how nuclear inclusion formation is linked to neurodegeneration.[4]

It is still under debate whether nuclear inclusions are associated with accelerated neurodegeneration, or whether they may have a protective function. If nuclear inclusion formation leads to neurodegeneration, it is expected that each individual neurone would show shrinkage once it harbours nuclear inclusions. It is therefore essential to identify possible morphological changes in neurones and their relation to nuclear inclusions in human brains obtained at necropsy. This is the first morphometric study on SCA1 designed to examine the influence of nuclear inclusions on nuclear size and deformity in human brains.

METHODS

We examined brains obtained at necropsy from seven Japanese cases of SCA1 and five controls without neurological disorders. Three of the seven SCA1 cases were from the same family. Clinical and pathological features of the SCA1 cases were compatible with the disease, and the diagnosis was also confirmed by genetic analysis.

Formalin fixed, paraffin embedded sections (6 μm thick) were obtained from the mid-pons. Pontine nuclei were chosen for this analysis because of the homogeneous size and character of the neurones in the pons, which makes it easier to quantify and interpret morphological alterations. The high frequency of nuclear inclusions in pontine neurones is another advantage for estimating their possible influence. The sections from the pons contained no localised foci of ischaemia or gliosis.

Deparaffinised sections from the SCA1 cases were immunostained with an antiubiquitin antibody (rabbit polyclonal, 1:1000; Dako, Glostrup, Denmark), with diaminobenzidine as a chromogen, and were then stained lightly with haematoxylin. Ten rectangular microscopic fields ($400 \times 250\ \mu m^2 = 0.1\ mm^2$) were chosen at random and captured by a digital camera connected to a microscope. Large cells harbouring Nissl

Abbreviations: CI, circularity index; DRPLA, dentatorubral-pallidoluysian atrophy; NIHID, neuronal intranuclear hyaline inclusion disease; NI+, nuclear inclusions present; NI–, nuclear inclusions absent; SCA1, spinocerebellar ataxia type 1

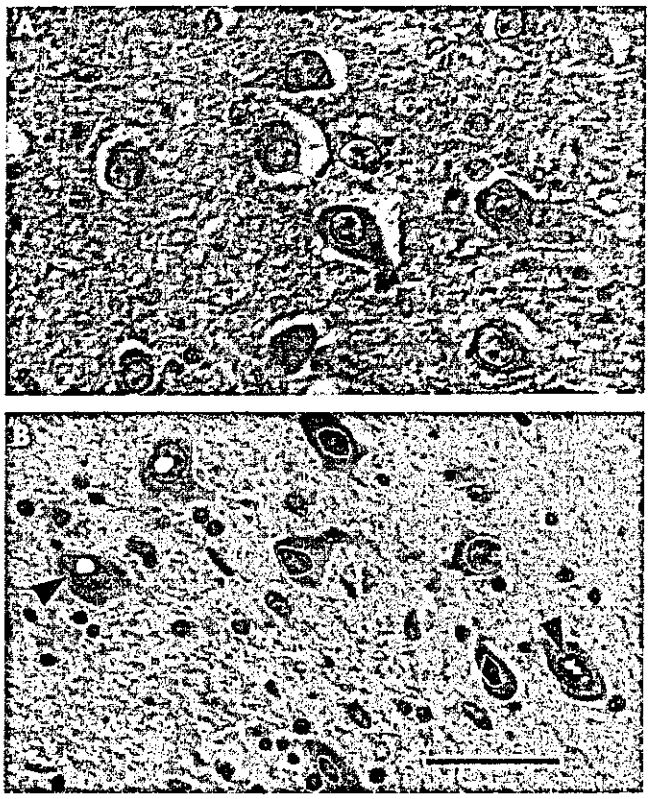

Figure 1 Pontine neurones from a control case (panel A, haematoxylin-eosin stain) and a case of spinocerebellar ataxia type 1 (SCA1) (panel B, ubiquitin immunostain counterstained with haematoxylin). The contour of the nucleus of each neurone is traced in black (in panel A, and neurones with nuclear aggregates in panel B) or in white (neurones without nuclear inclusions in panel B). Undulations of the nuclear membrane are conspicuous (arrowheads in panel B) in SCA1 neurones. Ubiquitin immunopositive nuclear inclusions are indicated as white spots in panel B.

substances and nuclei containing identifiable nucleoli or ubiquitin immunopositive nuclear inclusions were identified as neurones. Every field contained neurones with and without nuclear inclusions.

The contours of the nuclear membrane in each neurone and of the nuclear inclusions, if present, were traced on a digitiser coupled to a liquid crystal display (PL-400, Wacom, Saitama, Japan). Examples are shown in fig 1. "Nuclear area," "perimeter," "long axis," and "short axis" from the traced nuclear contours, and "nuclear inclusion area" from the traced nuclear inclusion contours, were calculated using NIH-Image (version 1.62). Because an increase in nuclear size is attributable to the presence of nuclear inclusions, nuclear area not occupied by nuclear inclusions ([nuclear area – nuclear inclusion area]) was also analysed. Nuclear deformity was assessed by the long axis/short axis ratio and "circularity index" (CI), defined by the ratio of two diameters, one of which is estimated from the perimeter (perimeter/2π) and the other from the area ($\sqrt{[\text{area}/\pi}$). CI = 1 if the traced nuclear contour is an exact circle. An increase in the long axis/short axis ratio or CI is correlated with the severity of nuclear deformities (elongation, distortion, or undulations of the nuclear membrane).

Statistics

Differences in the variables between groups with nuclear inclusions (NI+) and groups without nuclear inclusions (NI–) from both SCA1 cases (SCA1 total group, including both NI+ and NI– groups) and controls were estimated by analysis of variance (ANOVA) or Student's *t* test.

RESULTS

Table 1 shows the demographic data on the patients and the neuronal count of each case. The mean of the neuronal counts (representing the mean packing density) of the SCA1 group (83.9/mm²) was significantly smaller than that of the controls (160.2/mm², $p < 0.01$; Mann–Whitney U test).

The morphological data assembled from each group are shown in table 2. Nuclear area, perimeter, and short axis were significantly smaller in the SCA1 total group than in the controls (for example, the mean nuclear area was 81.4 μm² in the SCA1 group *v* 90.5 μm² in the control group; $p < 0.0001$ by Student's *t* test).

The inverted histograms in fig 2 show that the size distribution (nuclear area) of the SCA1 total group (filled bars) was smaller than that of the controls (unfilled bars). Nuclear shrinkage (estimated by nuclear area, perimeter, long axis, and short axis) was more profound in the NI– group than in the NI+ group, or the neuronal nuclei in the NI+ group were less atrophic than in the NI– group ($p < 0.0001$ by ANOVA, PLSD (protected least significant difference) of Fisher at 1% probability). The upper histograms in fig 2 show the difference in nuclear area between the NI+ group (unfilled bars) and the NI– group (filled bars).

There was no difference between the NI+ group and the NI– group in [nuclear area – nuclear inclusion area], neither was there a significant correlation between nuclear inclusion area and nuclear area, as shown in the scattergram in fig 3

Table 1 Neuronal counts (/mm²) with and without nuclear inclusions

Case	Age at onset/death (years)	Sex	Inclusions present (n/mm²)	Inclusions absent (n/mm²)	Total
SCA1 case 1	39/55	F	24	71	95
SCA1 case 2	41/50	M	29	67	96
SCA1 case 3	41/55	F	32	62	94
SCA1 case 4	30/50	F	23	67	90
SCA1 case 5	46/63	F	14	40	54
SCA1 case 6	37/48	M	23	49	72
SCA1 case 7	46/66	M	12	74	86
Mean					83.9*
Control	/25	M	0	140	140
Control	/25	F	0	174	174
Control	/40	F	0	154	154
Control	/44	M	0	157	157
Control	/45	F	0	176	176
Mean					160.2

*Significantly smaller than the control group ($p < 0.01$; Mann–Whitney U test).
F, female; M, male; SCA1, spinocerebellar ataxia type 1.

Table 2 Morphometric indices of pontine neurones in control and SCA1 cases

Index	Controls (n=5)	SCA1 (n=7) Total	NI+	NI–
Number of neurones	801	587	157	430
Nuclear area (μm²)	90.5 (19.8)	81.4 (21.8)*	87.2 (24.4)	79.2 (20.4)***¶
[Nuclear area minus nuclear inclusion area]		78.0 (21.4)*	74.5 (23.6)***	79.2 (20.4)***
Perimeter (μm)	36.3 (4.0)	34.4 (4.5)*	35.8 (4.9)	34.0 (4.3)***¶
Long axis (μm)	12.00 (1.48)	11.77 (1.72)	12.09 (1.71)	11.65 (1.71)**†
Short axis (μm)	9.54 (1.25)	8.71 (1.48)*	9.06 (1.69)***	8.58 (1.37)***¶
Long axis/short axis ratio	1.27 (0.18)	1.38 (0.25)*	1.37 (0.25)***	1.38 (0.25)***
Circularity index	1.085 (0.037)	1.088 (0.040)	1.095 (0.048)**	1.086 (0.037)

Values are expressed as mean (SD).
*p < 0.0001 v control group (Student's *t* test).
**p < 0.01, ***p < 0.0001 v control group; ¶p ≤ 0.0001 v NI+ group; †p < 0.01 v NI+ group (ANOVA, PLSD of Fisher at 1% probability).
ANOVA, analysis of variance; NI+, neurones with nuclear aggregates from SCA1 cases; NI–, neurones without nuclear aggregates from SCA1 cases, PLSD, protected least significant difference; SCA1, spinocerebellar ataxia type 1; total, all neurones from SCA1 cases.

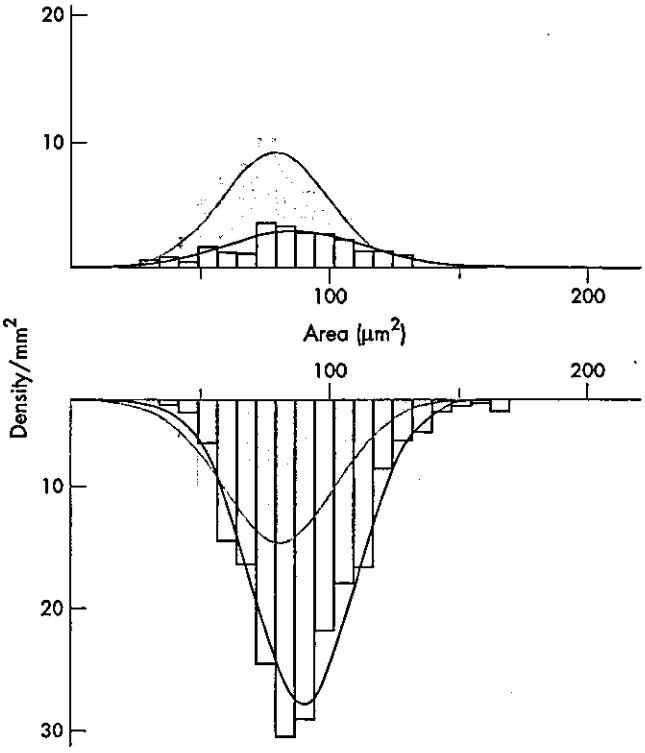

Figure 2 Size distribution of the nuclear size of the pontine neurones from cases with spinocerebellar ataxia type 1 (SCA1) and control cases. Nuclear size estimated as nuclear area in μm² is expressed along the abscissa. The ordinate represents relative frequency of each size expressed as density/mm². The lower inverted histograms refer to the controls (unfilled bars and a black line) and to the SCA1 total group (filled bars and a grey line). The upper histograms refer to the SCA1 group without nuclear inclusions (filled bars and a grey line), and to the SCA1 group with nuclear inclusions (unfilled bars and a black line).

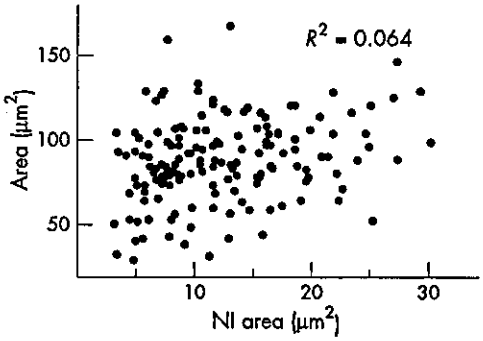

Figure 3 Absence of correlation (R^2 = 0.064) between nuclear size ("area" in μm² along the ordinate) and nuclear inclusion size ("NI area" in μm² along the abscissa).

(R^2 = 0.064). Furthermore, there were no significant correlations between age at onset or duration of illness and any of the morphological variables, including nuclear area (data not shown).

Although the value for long axis was not statistically different between the SCA1 total group and the controls, it was significantly smaller in the NI– group than in the NI+ group. The long axis/short axis ratio—one of the indices of nuclear deformity—was increased in both the SCA1 groups compared with the controls, but with no significant difference between the NI+ and the NI– groups. CI, another index of nuclear deformity, was significantly increased in the NI+ group compared with the controls, but the CI value in the NI– group was similar to that in the control group (fig 4).

DISCUSSION

In this study we investigated whether the presence of nuclear inclusions was linked to morphological changes in neurones during neurodegeneration in human brains obtained at necropsy. Unexpectedly, we found that nuclear shrinkage of the pontine neurones in brains from SCA1 patients was attenuated when nuclear inclusions were present. Nuclear inclusions are a pathological hallmark for most of the CAG/polyglutamine repeat disorders, including SCA1, and are composed of the protein altered by the expansion of CAG/polyglutamine tracts. These altered proteins have therefore been considered to be a link between neurodegeneration and nuclear inclusion formation, although the precise relation between nuclear inclusions and neurodegeneration is still unclear. On the other hand, cellular atrophy—which is considered to represent a stage preceding cell death—is a principal feature of neurodegeneration regardless of its aetiology, because degenerative processes in general develop slowly and usually take several years or even decades.

The nuclear shrinkage in pontine neurones of the SCA1 cases observed in our study indicated that cellular atrophy was the pathological feature representing the neurodegenerative process in this condition. Sorting the neurones into those with and without nuclear inclusions further clarified the situation, in that we could show that neurones with nuclear inclusions were *less* atrophic than those without. This result, from human brains obtained at necropsy, is not compatible with the hypothesis that the neurodegenerative process is accelerated in the presence of nuclear inclusions.

Studies carried out both in vitro and in vivo have provided conflicting evidence about the possible role of nuclear inclusion

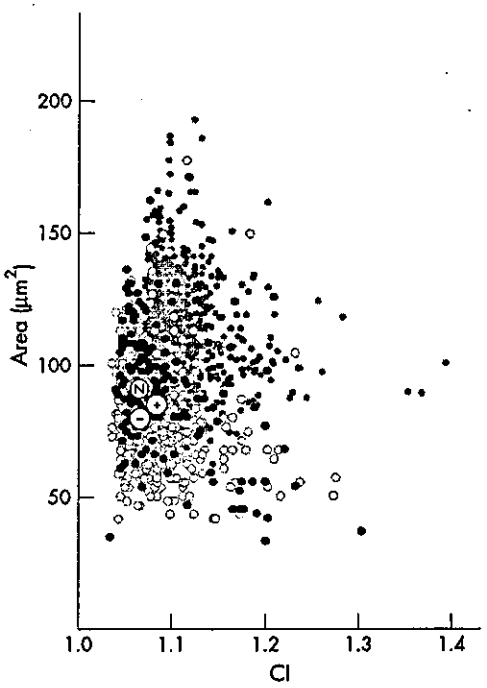

Figure 4 Relation between nuclear size ("area" along the ordinate in μm²) and deformity of the nucleus (circularity index (CI) along the abscissa). CI = 1 if the nucleus is an exact circle and increases if the nucleus is deformed by elongation or undulation. Grey dots = normal group; black dots = NI+ group; white dots = NI− group. Mean values for each group are plotted within larger circles as: N (normal group), − (NI− group), and + (NI+ group) in the scattergram. NI, nuclear inclusions.

formation and its relation to neurodegeneration. Neurodegeneration and nuclear inclusion formation in transgenic models of Huntington's disease are induced by the continued expression of the huntingtin fragment, carrying expanded polyglutamine,[5] and are possibly reduced by inhibition of caspase-1.[6] However, the suppression of nuclear inclusion formation by a caspase inhibitor did not increase neuronal survival in cultured cells transfected with the huntingtin gene carrying an expanded CAG repeat.[7] In cultured cells transfected with mutant huntingtin, blocking ubiquitination led to decreased nuclear inclusion formation and accelerated cell death.[8] This discrepancy is reflected in the observation that transgenic mice expressing mutant ataxin-1 without the self association domain develop a pathological phenotype without forming nuclear inclusions.[9]

Necropsy observations on human brains from patients with Huntington's disease[10] or neuronal intranuclear hyaline inclusion disease (NIHID)[11] showed a similar discrepancy between neuronal depletion and nuclear inclusion formation. At least two entirely opposing interpretations have been proposed to explain these data. If the presence of nuclear inclusions correlates with mutant protein induced cell death, atrophic features may be more exaggerated in neurones containing nuclear inclusions than in those without. The other possibility is that nuclear inclusion formation may be part of a process linked to the protection of cells from the toxic effects of the mutant protein. In that case we may expect that neurones without nuclear inclusions would show more atrophic features. The former possibility is not in agreement with what we observed in pontine neurones of the SCA1 brains in the present study, because neuronal nuclei containing nuclear inclusions were not smaller than those without, though pontine neurones of SCA1 brains—regardless of the presence of nuclear inclusions—were more atrophic than control brains.

When "nuclear inclusion area" was subtracted from "nuclear area," the size of neuronal nuclei in the NI+ group did not differ from that in the NI− group. However, nuclear inclusion size was not correlated with nuclear area. This means that the influence of nuclear inclusions on nuclear area—even if the inclusions were inserted from the extranuclear compartment—does not solely reflect the simple addition of "nuclear inclusion area." Nuclear inclusions may in fact be formed in the nucleus rather than being inserted from extranuclear compartments. In that case, a fraction of the nucleus is altered into nuclear inclusions, in which case one might expect that [nuclear area − nuclear inclusion area] would be decreased by the size of the nuclear inclusions. Our morphometric study, however, showed that the decrease in [nuclear area − nuclear inclusion area] in the NI+ group relative to the NI− group (79.2 μ^2 − 74.5 μ^2 = 4.7 μ^2) was less than half the nuclear inclusion area itself (87.2 μ^2 − 74.5 μ^2 = 12.7 μ^2). If nuclear inclusion formation were linked to some mechanism accelerating degeneration, the decrease in [nuclear area − nuclear inclusion area] should have exceeded the nuclear inclusion area. The present study showed, on the contrary, that this decrease was much attenuated. This attenuated decrease is explicable if nuclear size as a whole is increased during nuclear inclusion formation, as we demonstrated in this study.

A recent morphometric study showed that in dentatorubral-pallidoluysian atrophy (DRPLA), cerebellar granule cells containing nuclear inclusions were larger than those that did not.[12] Our recent morphometric study on pontine neurones from Machado-Joseph disease brains showed that [nuclear area − nuclear inclusion area] of NI+ neurones was significantly larger than that of NI− neurones.[13] Furthermore, it was even larger in NIHID than in normal controls.[14] In these disorders, NI+ neurones were in general less atrophic than NI− neurones, raising the possibility that neurones are equipped with common machinery triggered by or accompanied by nuclear inclusion formation and possibly counteracting polyglutamine induced neurodegeneration. However, the influence of nuclear inclusions on nuclear size is variable depending on the disease involved, and they appear to have a relatively less pronounced influence in SCA1. If this were not the case, the atrophic process in SCA1 might be so profound as to overwhelm this possible counteracting factor.

While it is generally recognised that CAG repeat length relates to the severity of illness and the age of onset, the age at onset of the SCA1 cases in this study was restricted within the range of 30 to 46 years and there was no significant correlation between the age at onset and the different variables that we examined. Larger numbers of cases with a broader age range of onset might have identified a possible influence of age on morphological change in the two groups of neurones. However, it may be that age at onset is not a major determinant for nuclear inclusion formation and neuronal atrophy.

In the present study, a fraction of neurones that actually contained nuclear inclusions might have been falsely classified into the NI− group because our observation on a two dimensional plane may have failed to detect nuclear inclusions that were not included in the plane of the 6 μm thick sections. If neurones with nuclear inclusions were smaller than those without nuclear inclusions, this possible failure to identify inclusions not recognised in the two dimensional plane might have led to underestimation of the size of the neurones in the NI− group. However, because the present study indicated the opposite—that is, it showed that neuronal nuclei in the NI+ group were *larger* than those in the NI− group—it is reasonable to conclude from this two dimensional study that neuronal nuclei with nuclear inclusions are significantly larger than neuronal nuclei without nuclear inclusions.

Our study showed an increase in the long axis/short axis ratio in the SCA1 group and an increase in CI in the NI+ group compared with the controls, without an increase in CI in the NI− group. This suggests that the nuclei of pontine neurones in SCA1 are deformed, and especially those with nuclear

inclusions. One would expect these deformities to be secondary to nuclear shrinkage. The larger nuclear size of the NI+ group, however, was associated with a more marked increase in the indices of nuclear deformity, which indicates that a mechanism other than nuclear shrinkage could be one of the determinants of these deformities. These deformities might otherwise be influenced by the presence of nuclear inclusions in SCA1 brains. An apparent indentation of the nuclear membrane may be observed even in normal neurones,[15] and a pathological increase in this indentation has been described in human brains with DRPLA[12] and Huntington's disease,[16] and in an animal model.[17] Although our present observations, based on light microscopy, failed to identify deep indentations of the nuclear membrane, an increase in the long axis/short axis ratio in SCA1 neurones and an increase in the circularity index in SCA1 neurones with nuclear inclusions may represent similar pathological changes. These would be common to the CAG/polyglutamine repeat disorders and would be partly independent of nuclear atrophy, as we demonstrated in SCA3 and NIHID brains.[12 13]

Although it is evident that both nuclear inclusion formation and neuronal degeneration are induced by an expanded CAG repeat, our study shows that the presence of nuclear inclusions does not necessarily parallel the extent of neurodegeneration, as measured by nuclear size. Rather, the presence of nuclear inclusions was associated with an incease in the size of the neuronal nuclei, which does not support the hypothesis that the inclusions are linked to accelerated neurodegeneration. Cellular mechanisms linking nuclear inclusion formation and neurodegeneration, however, remain elusive. One possibility is that the ubiquitin–proteasome pathway is involved in both neuroprotection and nuclear inclusion formation. Downregulation of ubiquitin–proteasome pathway has been found to suppress nuclear inclusion formation and to accelerate cell death in parallel in studies carried out in vitro.[18] This inverse relation between cell death and nuclear inclusion formation through the ubiquitin–proteasome pathway suggests that nuclear inclusion formation is linked to a possible intrinsic neuroprotective mechanism mediated by ubiquitin. We have shown that ubiquitin is commonly localised to the periphery of nuclear inclusions in brains from patients with Machado-Joseph disease[19] and NIHID.[20]. These findings are explicable if nuclear inclusion formation mediated by ubiquitin is associated with a mechanism counteracting neuronal shrinkage, as was reported in SCA1 transgenic mice.[21] Further investigation into the relation between nuclear inclusion formation and cellular atrophy will clarify whether these morphological features and their interpretation are shared with other conditions characterised by nuclear inclusions, and will determine whether nuclear inclusions serve as a morphological hallmark for polyglutamine induced neurodegeneration or neuroprotection. Furthermore, clarification of the molecular mechanism of nuclear inclusion formation will give a rational basis for a therapeutic strategy that may retard or even reverse neurodegeneration by activating or modulating this machinery.

ACKNOWLEDGEMENTS

This work was supported partly by grants from the Ministry of Health and Welfare (KI) and from Japan Society for the Promotion of Science/INSERM (TU).

Authors' affiliations
U Nagaoka, Department of Neurology, Tokyo Metropolitan Neurological Hospital, Tokyo, Japan
U Nagaoka, T Uchihara, Department of Neuropathology, Tokyo Metropolitan Institute for Neuroscience
N Funata, Department of Pathology, Tokyo Metropolitan Komagome Hospital
K Iwabuchi, Department of Neurology and Psychiatry, Kanagawa Rehabilitation Centre, Atsugi, Japan
S Yagishita, Department of Pathology, Kanagawa Rehabilitation Centre
H Konno, Department of Neurology, National Sanatorium Nishitaga Hospital, Miyagi, Japan
M Tobita, Department of Neurology, Miyagi National Hospital
T Kato, Third Department of Internal Medicine, Yamagata University School of Medicine, Yamagata, Japan

Competing interests: none declared

REFERENCES

1 **Orr HT,** Chung MY, Banfi S, *et al.* Expansion of an unstable trinucleotide CAG repeat in spinocerebellar ataxia type 1. *Nat Genet* 1993;4:221–6.
2 **Zoghbi HY,** Orr HT. Glutamine repeats and neurodegeneration. *Annu Rev Neurosci* 2000;23:217–47.
3 **Kaytor M,** Warren S. Aberrant protein deposition and neurological disease. *J Biol Chem* 1999;274:37507–10.
4 **Sisodia SS.** Nuclear inclusions in glutamine repeat disorders: are they pernicious, coincidental, or beneficial? *Cell* 1998;95:1–4.
5 **Yamamoto A,** Lucas JJ, Hen R. Reversal of neuropathology and motor dysfunction in a conditional model of Huntington's disease. *Cell* 2000;101:57–66.
6 **Ona VO,** Li M, Vonsattel JP, *et al.* Inhibition of caspase-1 slows disease progression in a mouse model of Huntington's disease. *Nature* 1999;399:263–7.
7 **Kim M,** Lee H-S, LaForet G, *et al.* Mutant huntingtin expression in clonal striatal cells: dissociation of inclusion formation and neuronal survival by caspase inhibition. *J Neurosci* 1999;19:964–73.
8 **Saudou F,** Finkbeiner S, Devys D, *et al.* Huntingtin acts in the nucleus to induce apoptosis but death does not correlate with the formation of intranuclear inclusions. *Cell* 1998;95:55–66.
9 **Klement IA,** Skinner PJ, Kaytor MD, *et al.* Ataxin-1 nuclear localization and aggregation: role in polyglutamine-induced disease in SCA1 transgenic mice. *Cell* 1998;95:41–53.
10 **Kuemmerle S,** Gutekunst C-A, Klein AM, *et al.* Huntingtin aggregates may not predict neuronal death in Huntington's disease. *Ann Neurol* 1999;46:842–9.
11 **Takahashi J,** Tanaka J, Arai K, *et al.* Recruitment of non-expanded polyglutamine proteins in intranuclear aggregates of neuronal intranuclear hyaline inclusion disease. *J Neuropathol Exp Neurol* 2001;60:369–76.
12 **Takahashi H,** Egawa S, Piao Y-S, *et al.* Neuronal nuclear alterations in dentatorubral-pallidoluysian atrophy: ultrastructural and morphometric studies of the cerebellar granule cells. *Brain Res* 2001;919:12–19.
13 **Uchihara T,** Iwabuchi K, Funata N, *et al.* Attenuated nuclear shrinkage in neurons with nuclear aggregates – a morphometric study on pontine neurons of Machado-Joseph disease brains. *Exp Neurol* 2002;178:124–8.
14 **Uchihara T,** Tanaka J, Funata N, *et al.* Influence of intranuclear inclusion on nuclear size – morphometric study on pontine neurons of neuronal intranuclear inclusion disease cases. *Acta Neuropathol* 2003;105:103–8.
15 **Roos RAC,** Bots GTAM. Nuclear membrane indentations in Huntington's chorea. *J Neurol Sci* 1983;61:37–47.
16 **Bots GTAM,** Bruyn GW. Neuropathological changes of the nucleus accumbens in Huntington's chorea. *Acta Neuropathol* 1981;55:21–2.
17 **Davies SW,** Turmaine M, Cozens BA, *et al.* Formation of neuronal intranuclear inclusions underlies the neurological dysfunction in mice transgenic for the HD mutation. *Cell* 1997;90:537–48.
18 **Cummings CJ,** Reinstein E, Sun Y, *et al.* Mutation of the E6-AP ubiquitin ligase reduces nuclear inclusion frequency while accelerating polyglutamine-induced pathology in SCA1 mice. *Neuron* 1999;24:879–92.
19 **Fujigasaki H,** Uchihara T, Koyano S, *et al.* Ataxin-3 is translocated into the nucleus for the formation of intranuclear inclusions in normal and Machado-Joseph disease brains. *Exp Neurol* 2000;165:248–56.
20 **Takahashi J,** Fukuda T, Tanaka J, *et al.* Neuronal intranuclear hyaline inclusion disease with polyglutamine immunoreactive inclusions. *Acta Neuropathol* 2000;99:589–94.
21 **Cummings CJ,** Mancini MA, Antalffy B, *et al.* Chaperone suppression of aggregation and altered subcellular proteasome localization imply protein misfolding in SCA1. *Nat Genet* 1998;19:148–54.

Acta Neuropathol (2003) 105 : 508–514
DOI 10.1007/s00401-003-0675-4

REGULAR PAPER

Katsuhiko Shibuya · Toshiki Uchihara · Ayako Nakamura
Miyako Ishiyama · Keiko Yamaoka · Saburo Yagishita
Kiyoshi Iwabuchi · Kenji Kosaka

Reversible conformational change of tau2 epitope on exposure to detergent in glial cytoplasmic inclusions of multiple system atrophy

Received: 14 October 2002 / Revised: 18 December 2002 / Accepted: 18 December 2002 / Published online: 26 February 2003
© Springer-Verlag 2003

Abstract Tau-like immunoreactivity (IR) on glial cytoplasmic inclusions (GCIs) of multiple system atrophy (MSA) was investigated with a panel of anti-tau antibodies and we found that tau2, one of the phosphorylation-independent antibodies, preferentially immunolabeled GCIs. Co-presence (0.03%) of polyethyleneglycol-*p*-isooctylphenyl ether (Triton X-100, TX) with tau2, however, abolished this IR on GCIs, but did not abolish tau2 IR on neurofibrillary tangles (NFTs). Tau2-immmunoreactive bands on immunoblot of brain homogenates from MSA brains were retrieved mainly in a TRIS-saline-soluble fraction, as reported in normal brains. This was in contrast to SDS-soluble fractions from brain with Down's syndrome, which contained tau2-immuoreactive bands of higher molecular weight. It indicates that the appearance of tau2 IR on GCIs is not related to hyperphosphorylation of tau. These tau2-immunoreactive bands, except those from bovine brain, were similarly abolished in the presence of TX (0.06%), and repeated washing after exposure to TX restored the tau2 IR on immunohistochemistry and on immunoblot. These findings can be explained if the modified tau2 epitope undergoes a reversible conformational change on exposure to TX, which is reversible after washing. Because the conformation centered at Ser101 of bovine tau is crucial for its affinity to tau2, the Ser-like conformation mimicked by its human counterpart Pro may represent pathological modification of tau shared by GCIs and NFTs. The relative resistance of tau2 epitope on NFTs on exposure to TX suggests that tau woven into NFTs confers additional stability to the pathological conformation of tau2 epitope. The conformation of the tau2 epitope in GCIs is not as stable as in NFTs, suggesting that tau proteins are not the principal constituents of the fibrillary structures of GCIs, even though they were immunodecorated with tau2. The difference in the susceptibility of the tau2 epitope to TX may distinguish its conformational states, which are variously represented according to disease conditions.

Keywords Tau2 epitope · Conformational change · Reversible · Detergent · Glial cytoplasmic inclusions

K. Shibuya · K. Iwabuchi
Department of Neurology and Psychiatry,
Kanagawa Rehabilitation Center,
516 Nanasawa Atsugi-shi, 243-0121 Kanagawa-ken, Japan

K. Shibuya · T. Uchihara (✉) · A. Nakamura
Department of Neuropathology,
Tokyo Metropolitan Institute for Neuroscience,
2-6 Musashi-dai, Fuchu, 183-8526 Tokyo, Japan
Tel.: +81-42-3253881 ext 4712, Fax: +81-42-3218678,
e-mail: uchihara@tmin.ac.jp

M. Ishiyama · K. Yamaoka · S. Yagishita
Department of Pathology, Kanagawa Rehabilitation Center,
516 Nanasawa Atsugi-shi, 243-0121 Kanagawa-ken, Japan

K. Kosaka
Department of Psychiatry,
Yokohama City University School of Medicine,
3-9 Fukuura, Kanazawa-ku, 236-0004 Yokohama, Japan

Introduction

Multiple system atrophy (MSA) includes olivopontocerebellar atrophy, striatonigral degeneration and Shy-Drager syndrome [11]. Argyrophilic oligodendroglial cytoplasmic inclusions (GCIs) are the pathological hallmark of MSA [19, 24]. GCIs are immunostained with antibodies against ubiquitin [13, 15, 18, 23, 25, 27, 31], α-synuclein [5, 32, 36], tubulin [1, 13, 19, 23, 24], microtubule-associated proteins (MAPs) [1, 15, 29], αB-crystallin [18, 31] and Rosenthal fiber protein [13]. Tau-like immunoreactivity (IR) on GCIs has been, however, inconsistently reported as being positive [1, 15, 24, 27], weak [13, 18], partial [29], dependent on the antibody [8] or negative [2, 19]. We tested a panel of anti-tau antibodies to look for possible immunolocalization of tau in MSA brains, and its relation to GCIs. We found that tau2, one of the phosphorylation-independent antibodies, consistently immunolabeled GCIs, while other anti-tau antibodies failed to immunolabel GCIs. Selective visualization of tau2 epitope not associated with that of other tau epitopes on GCIs

is similar to that was observed on microglial cell around ischemic foci [20, 34, 35], and is distinct from neurofibrillary tangles (NFTs). Moreover, we became aware that tau2 IR on these microglial cells was abolished when tau2 was diluted with buffers containing polyethyleneglycol-*p*-isooctylphenyl ether (Triton X-100, TX; WAKO, Tokyo, Japan), a detergent frequently used for immunodetection procedures [35]. The immunohistochemical similarity of GCIs to microglia around ischemic focus prompted us to examine possible influences of TX on tau2 IR of GCIs using immunohistochemistry and immunoblot on a series of brains from MSA patients obtained at autopsy. The influence of TX on tau2 IR, as we demonstrated in the present study, may represent a possible change in conformational state of tau2 epitope, modified differently according to disease conditions.

Materials and methods

We examined the cerebella and putamens of five pathologically diagnosed cases of MSA (four males and one female, average age at death: 64.6±5.9 years and duration of illness: 6.8±2.7 years, expressed as mean±SD) as shown in Table 1 and the hippocampus from a case of Down's syndrome (DS) with neuropathological features of Alzheimer's disease.

Immunohistochemistry

The formalin-fixed slices of the cases were embedded in paraffin and 5-μm-thick sections were obtained. A panel of anti-tau antibodies included tau1 (1:5,000, Boehringer, Mannheim, Germany) [22], tau2 (1:1,000, Sigma, St Louis, Mo.) [22], anti-human tau (pool 2, 1:10,000, a generous gift from Professor Y. Ihara, University of Tokyo) [9], Alz-50 (1:200, a generous gift from Professor Davies, Albert Einstein University) [38], anti-PHF monoclonal AT8 (1:10,000, Innogenetics, Zwijindrecht, Belgium) [17]. Epitopes were visualized using the ABC method with diaminobenzidine and nickel ammonium sulfate as a chromogen. Influence of Triton X-100 (TX) on tau2 IR was examined by incubating deparaffinized sections overnight at 4°C with tau2 diluted in phosphate-buffered saline (PBS) containing various concentrations (0.3%, 0.03%, 0.003%, 0%) of TX. Possible restoration of tau2 IR, once disappeared on exposure to TX, was tested by incubating the sections initially with PBS containing 0.03% TX overnight. Before being subjected to tau2 immunohistochemistry, these sections were washed for 10 min either once, twice or three times with PBS not containing TX. They were then processed in parallel by incubating with tau2 diluted in PBS not containing TX. The subsequent immunohistochemical procedures were the same as above. The sections from MSA and DS cases were subjected to immunohistochemistry with other anti-tau antibodies. The antibodies were diluted either with PBS containing 0.03% TX or with that not containing TX. Treatment with alkaline phosphatase was performed prior to immunohistochemistry with tau1, and the efficacy of the pretreatment was confirmed when AT8 IR on NFTs disappeared after the treatment [17].

Table 1 Summary of cases of MSA

Case	Sex	Age at death (years)	Duration of illness (years)
1	M	59	3
2	M	71	4
3	M	59	8
4	F	62	9
5	M	72	10

Immunoelectron microscopy [12]

Fragments of cerebellar white matter were sampled from formalin-fixed blocks of MSA cases. They were re-fixed in 2.5% glutaraldehyde and thin frozen sections were made. After being blocked with normal goat serum, samples were incubated with tau2 (1:10) overnight. Secondary anti-mouse IgG nanogold (Nanopobes, Yaphank, N.Y.) diluted to1:20 was then applied for 5 h. The specimens were fixed in 1% glutaraldehyde. Gold particles were visualized by silver enhancement followed by gold-toning. The specimens were, then, post-fixed in 0.1% osmium tetroxide. Each section stained with toluidine blue was embedded in Epon. Ultrathin sections were double-stained with uranyl acetate and lead citrate, and observed under JOEL 2000FX electron microscope.

Fractionation of brains and immunoblotting

Small frozen pieces (0.5 g) from putamen of MSA, hippocampus of DS and bovine brain were homogenized in TRIS-buffered saline (TS, 50 mM TRIS, pH 7.6, 0.15 M NaCl). To minimize nonspecific proteolysis of tau, buffers were routinely prepared to contain 0.5 mM diisopropyl fluorophosphate, 0.5 mM phenylmethylsulfonyl fluoride, 1 μg/ml antipain, 0.1 μg/ml pepstatin and 1 μg/ml leupeptin. These samples were fractionated sequentially with TS, 1% Sarkosyl/TS buffer, 2% sodium dodecyl sulfate (SDS)/TS buffer and formic acid according to the method previously described [3, 9]. Soluble and insoluble fractions were separated by 200,000 *g* centrifugation for 20 min at 4°C except for SDS and formic acid extraction, which was carried out at room temperature.

The supernatant fraction of each homogenate was treated with the SDS sample buffer, heated at 95°C for 5 min and separated on 10% SDS-PAGE. Separated proteins in the gel were electrotransblotted onto a nitrocellulose membrane (Bio-Rad, Hercules, Calif.). After blocking with 5% nonfat dry milk in TRIS-buffered saline (TBS, 0.02 M TRIS-HCl, pH 7.6, 0.15 M NaCl), the membranes were incubated with tau2 (1:2,000) in the presence or absence of 0.06% TX for 1 h at room temperature. Membranes were then washed with TBS and incubated with horseradish peroxidase (HRP)-conjugated anti-mouse IgG (1:4,000, Kirkegaard and Perry, Gaithersburg, Md.) and visualized by the enhanced chemiluminescence (ECL) procedure as described by the manufacturer (Amersham, UK). The HRP activity remaining on the membrane was then inactivated by incubating it for 20 min with 2% hydrogen peroxide in TBS. After being blocked with 5% nonfat dry milk in TBS, the membrane was reprobed with an anti-human tau antibody (pool 2, 1:100,000). The membrane was then incubated with HRP-tagged anti-rabbit IgG (1:1,000, Pierce, Rockford, Ill.) for 2 h and subjected to ECL.

Possible restoration of tau2 IR, after its disappearance on exposure to TX, was tested by incubating the membranes initially with TBS containing 0.06% TX or in its absence for 1 h. Before probing with tau2, the membranes were washed for 3 h with TBS not containing TX. They were then probed in parallel by incubating with tau2 diluted in TBS not containing TX. The subsequent immunodetection procedures were the same as above.

Results

Immunohistochemistry

GCIs were clearly immunostained with tau2 when the sections were incubated with tau2 diluted in PBS not containing TX (Fig. 1A). This positive tau2 IR on GCIs was completely abolished (Fig. 1B) when the neighboring his-

tological section was incubated with tau2 and a synthetic peptide (AGIGDTS*NLEDQAA), which corresponded to the epitope of bovine tau. Ser101 of bovine tau, at the center of this synthetic peptide as indicated by the asterisk, was reported to be crucial for its affinity to tau2 and this Ser-like conformation, mimicked by its human counterpart Pro, represents pathological conformation of tau 2 epitope integrated in NFTs [37].

This tau2 IR on GCI (Fig. 2A) decreased when the sections were incubated with tau2 in the presence of 0.003% TX (Fig. 2B) and was completely abolished when the concentration of TX increased to 0.03 and 0.3% (Fig. 2C and D, respectively). Tau2 IR on NFTs of DS (Fig. 3A) was, in contrast, still evident even when tau2 was diluted in PBS containing 0.03% of TX (Fig. 3B).

Tau2 IR on GCIs (Fig. 4A) was abolished when the sections were incubated overnight with PBS containing 0.03% TX prior to immunostaining with tau2 diluted in PBS not containing TX (Fig. 4B). Washing the sections with PBS not containing TX, between the overnight incubation with 0.03% TX and the tau2 immunostaining, restored the tau2 IR (Fig. 4C, D). The more the sections were washed, the more intensely tau-2 IR was restored (Fig. 4C, D). Other anti-tau antibodies (tau1, human tau, Alz-50, AT8) failed to label GCIs. These anti-tau antibodies immunolabeled NFTs of DS, except that tau1 IR was detectable only after treatment with alkaline phosphatase.

Immunoelectron microscopy

GCIs consisted of a scattered fibrillary structure, approximately 10–15 nm in diameter. The gold granules were enhanced by silver, and immunodecorated the entire length of the fibrils (Fig. 5A, B).

Immunoblotting

Tau-immunoreactive bands were mainly detected by pool 2 in the TS-soluble fraction of MSA (Fig. 6A, lane 1), which was similarly visualized by tau2 (Fig. 6B, lane1). The molecular weight of these tau-immunoreactive bands from MSA brains was not different from normal tau. Tau-immunoreactive bands from DS brain were retrieved in the SDS-soluble fraction (Fig. 6C, lane 3) and they were of higher molecular weight.

Tau2-immunoreactive bands in TS-soluble fraction of MSA (Fig. 7A, lane 1) and those in SDS-soluble fraction of DS (Fig. 7A, lane2) were abolished when probed with tau2 diluted in TBS containing 0.06% TX (Fig. 7B). This was the minimum concentration which diminished tau2 IR in TS-soluble fraction of MSA. The membrane was prepared similarly, and was incubated with TBS containing 0.06% TX for 1 h and then washed for 3 h with TBS not containing TX. Subsequent probing with tau2 diluted with TBS not containing TX exhibited tau2-immunoreactive bands (Fig. 7C). TS-soluble fraction of MSA and SDS-soluble fraction of DS were similarly labeled with pool 2 (Fig. 7D, lanes 1 and 2). The TS-soluble fraction of bovine brain exhibited equivalent tau2 IR, even though it was diluted to 1:2,000 (Fig. 7, lanes 3). This tau2 IR retained even when tau2 was diluted with TBS containing 0.06% TX (Fig. 7B, lane 3).

Discussion

It has been debated and still remains to be settled whether tau-like IR is present in GCIs or not [1, 2, 13, 15, 18, 19,

Fig. 1 Tau2 IR on GCIs and its specificity. Tau2 IR on GCIs (A) was abolished on incubating the sections with tau2 diluted in buffer containing the specific blocking peptide (**B**) (*IR* immunoreactivity, *GCI* glial cytoplasmic inclusion). *Bar* 50 μm

Fig. 2 The influence of TX, dependent on its concentration, on tau-2 IR on histological sections from MSA. Sections from the cerebellum were immunolabeled with tau2 diluted in PBS containing different concentrations of TX (**A** 0%; **B** 0.003%; **C** 0.03%; **D** 0.3%). Tau-2 IR in GCIs (**A**) was diminished with increasing concentration of TX (**C**, **D**) (*TX* Triton X-100, *MSA* multiple system atrophy, *PBS* phosphate-buffered saline). *Bar* 50 μm

Fig. 3 Relative resistance of tau2 IR on NFTs. Neighboring sections from the hippocampus of brains with DS were immunostained with tau2 in the absence (**A**) or presence (**B**) of 0.03% TX. Tau-2 IR on NFTs was less influenced by the co-presence of TX than that on GCIs (Fig. 2) (*NFTs* neurofibrillary tangles, *DS* Down's syndrome). *Bar* 50 μm

Fig. 4 Disappearance of tau2 IR on GCIs on exposure to TX, and its restoration after washing. Neighboring sections from cerebellar white matter were immunostained with tau2 in the absence (**A**) of 0.03% TX. Those incubated with 0.03% TX were either not washed (**B**) or washed with PBS not containing TX once (**C**) or three times (**D**) prior to tau2 immunohistochemistry in the absence of TX. Tau-2 IR was restored after washing three times (**D**). *Bar* 50 μm

Fig. 5 Fibrils in GCIs immunodecorated by tau2. GCIs consisted of scattered fibrillary structures, approximately 10–15 nm in diameter, The gold granules, enhanced by silver, immunodecorated the entire length of the fibrils. *Bar* **A** 1,000 nm; **B** 500 nm

Fig. 6 Serially separated fractions (*lane 1* TS soluble; *lane 2* sarkosyl soluble; *lane 3* SDS soluble; *lane 4* formic acid-extracted) from homogenates of the MSA brain (**A**, **B**) and the DS brain (**C**) were subjected to 10% SDS-PAGE and probed with pool 2 (**A**) or tau2 (**B**, **C**). Pool 2-immunoreactive bands were mainly detected in the TS-soluble fraction of MSA (**A**, *lane 1*), which was similarly visualized by tau2 (**B**, *lane 1*), and SDS-soluble fraction of DS (**C**, *lane 3*) (*upper arrowhead*: 64 kDa: *lower arrowhead*: 50 kDa) (*TS* TRIS-buffered saline)

Fig. 7 Disappearance of tau2-immunoreactive bands on exposure to TX and their restoration after washing. TS-soluble fraction from the MSA brain (*lanes 1*), SDS-soluble fraction from the DS brain (*lanes 2*) and TS-soluble fraction from the bovine brain (diluted to 1:2,000, *lanes 3*) were subjected to 10% SDS-PAGE and probed with tau2 or pool 2. Tau2-immunoreactive bands, detectable when incubated with tau2 in the absence of TX (**A**), disappeared when incubated with tau2 in the presence of 0.06% TX (**B**). Tau2-immunoreative bands from the bovine brain were relatively resistant to exposure to TX (**B**, *lane 3*). Tau2-immunoreactive bands, disappeared on exposure to TX, were restored after washing performed prior to probing with tau2 (**C**). Fractions (**D**, *lanes 1* and *2*) were similarly labeled with pool 2, except for diluted TS fraction from bovine brain (**D**, *lane 3*) (*upper arrowhead*: 64 kDa: *lower arrowhead*: 50 kDa)

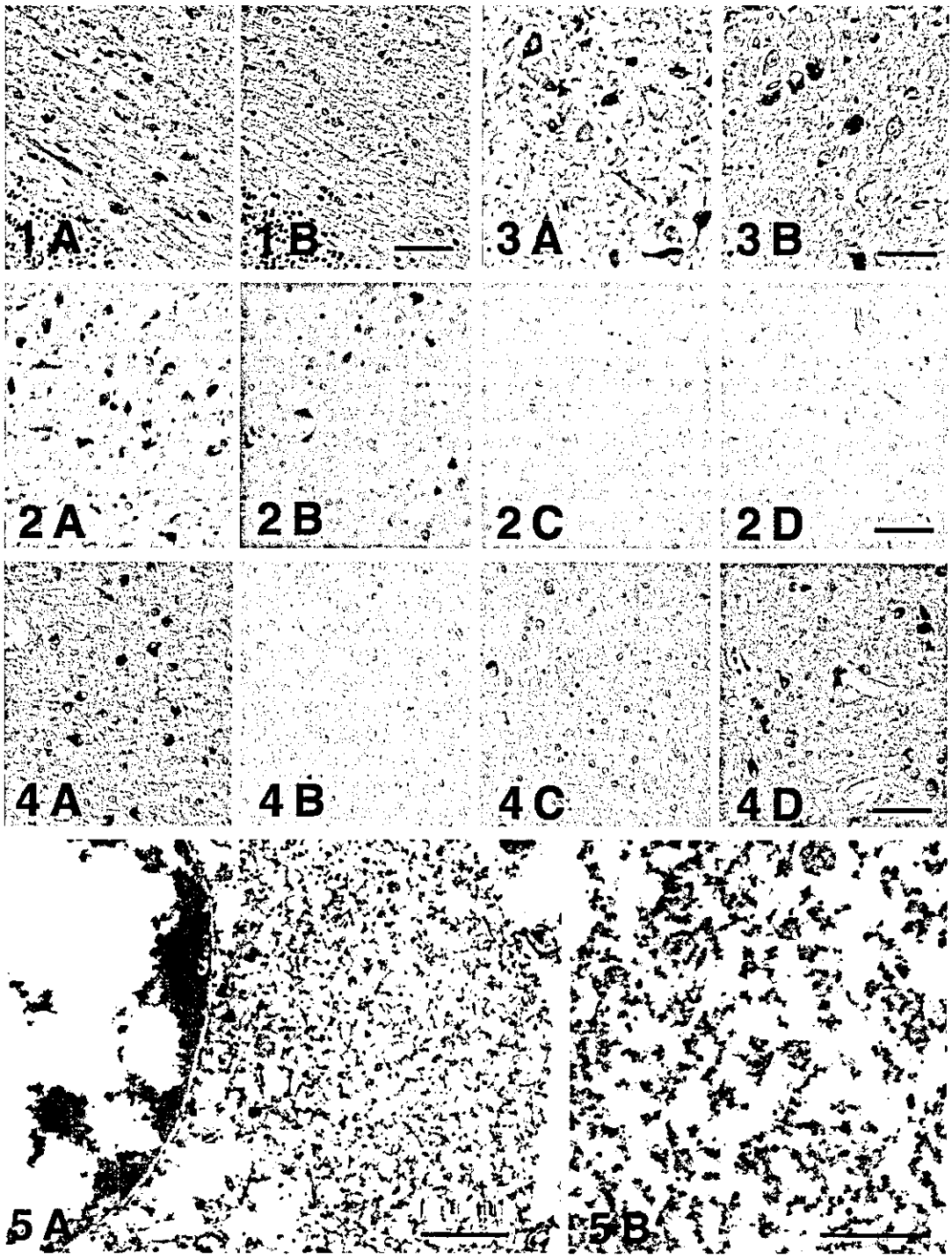
1A
1B
3A
3B
2A
2B
2C
2D
4A
4B
4C
4D
5A
5B

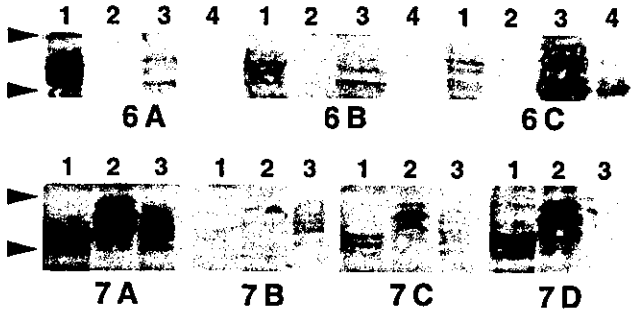
1 2 3 4 1 2 3 4 1 2 3 4
6A
6B
6C
1 2 3 1 2 3 1 2 3 1 2 3
7A
7B
7C
7D